Redox Biology 59 (2023) 102594

Contents lists available at ScienceDirect

Redox Biology

journal homepage: www.elsevier.com/locate/redox

Diminished α7 nicotinic acetylcholine receptor (α7nAChR) rescues amyloid-β induced atrial remodeling by oxi-CaMKII/MAPK/AP-1 axis-mediated mitochondrial oxidative stress

Jikai Zhao [a], Liming Yu [a], Xiaodong Xue [a], Yinli Xu [a], Tao Huang [a], Dengyue Xu [a,b], Zhishang Wang [a], Linyu Luo [a,c], Huishan Wang [a,*]

[a] Department of Cardiovascular Surgery, General Hospital of Northern Theater Command, No. 83, Wenhua Road, Shenhe District, Shenyang, PR China
[b] Postgraduate College, China Medical University, Shenyang, PR China
[c] Postgraduate College, Dalian Medical University, Dalian, PR China

ARTICLE INFO

Keywords:
α7nAChR
Atrial fibrillation
amyloid-β
Mitochondrial oxidative stress
Atrial remodeling
CaMKII

ABSTRACT

The potential coexistence of Alzheimer's disease (AD) and atrial fibrillation (AF) is increasingly common as aging-related diseases. However, little is known about mechanisms responsible for atrial remodeling in AD pathogenesis. α7 nicotinic acetylcholine receptors (α7nAChR) has been shown to have profound effects on mitochondrial oxidative stress in both organ diseases. Here, we investigate the role of α7nAChR in mediating the effects of amyloid-β (Aβ) in cultured mouse atrial cardiomyocytes (HL-1 cells) and AD model mice (APP/PS1). In vitro, apoptosis, oxidative stress and mitochondrial dysfunction induced by Aβ long-term (72h) in HL-1 cells were prevented by α-Bungarotoxin(α-BTX), an antagonist of α7nAChR. This cardioprotective effect was due to reinstating Ca^{2+} mishandling by decreasing the activation of CaMKII and MAPK signaling pathway, especially the oxidation of CaMKII (oxi-CaMKII). In vivo studies demonstrated that targeting knockdown of α7nAChR in cardiomyocytes could ameliorate AF progression in late-stage (12 months) APP/PS1 mice. Moreover, α7nAChR deficiency in cardiomyocytes attenuated APP/PS1-mutant induced atrial remodeling characterized by reducing fibrosis, atrial dilation, conduction dysfunction, and inflammatory mediator activities via suppressing oxi-CaMKII/MAPK/AP-1. Taken together, our findings suggest that diminished α7nAChR could rescue Aβ-induced atrial remodeling through oxi-CaMKII/MAPK/AP-1-mediated mitochondrial oxidative stress in atrial cells and AD mice.

1. Introduction

Both Alzheimer's disease (AD) and atrial fibrillation (AF) are age-depended diseases that frequently coexist [1]. The association between AD and AF is confirmed by epidemiological researches [2,3], and several studies have also considered AF can dramatically raise the risk of AD, which could mainly be explained by AF-induced cerebral hypoperfusion, oxidative injury and inflammatory disequilibrium [4,5]. The accumulation of amyloid-β (Aβ) deposition caused by abnormal cleavage of the amyloid precursor protein (APP) into pathological Aβ fragments is one of the pathological markers of AD [6]. The prevailing belief is that exacerbating Aβ accumulation and lowering Aβ clearance are the major determinants in the relationship of AD and AF [7]. Since AF could induce cognitive dysfunction leading to AD, the compromised cardiac function in AD patients, conversely, is still unclear. Recent evidence suggests that Aβ deposits are also present in myocardium of AD patients and contributes to myocardial dysfunction [8], indicating that Aβ might play a potential role in AF.

AF is the most common cardiac arrhythmia characterized by shortened atrial refractoriness and abnormal conduction [9], which may be related to abnormality of neural regulation [10] and myocardial fibrosis [11]. α7 nicotinic acetylcholine receptors (α7nAChR) responding to acetylcholine, a neurotransmitter from vagal nerve endings, plays a key role in regulating memory and cognitive function in central nervous system. In fact, Aβ can competitively combine with α7nAChR to exert neurotoxic effect, owing to the binding with high affinity between Aβ and α7nAChR [12,13]. Recent research demonstrated that Aβ is not

* Corresponding author. Department of Cardiovascular Surgery, General Hospital of Northern Theater Command, No. 83, Wenhua Road, Shenhe District, Shenyang, 110016, PR China.
E-mail address: huishanw@126.com (H. Wang).

https://doi.org/10.1016/j.redox.2022.102594
Received 9 May 2022; Received in revised form 15 October 2022; Accepted 28 December 2022
Available online 2 January 2023

Abbreviations

α7nAChR	α7 nicotinic acetylcholine receptors
α-BTX	α-Bungarotoxin
AAV	adeno-associated virus
Aβ	amyloid-β
AD	Alzheimer's disease
AF	atrial fibrillation
Ang II	angiotensin II
APP	amyloid precursor protein
AP-1	activator protein 1
CaMKII	calcium/calmodulin-dependent protein kinase II
CCK8	Cell Counting Kit-8
DHE	dihydroethidium
EF	ejection fraction
GSH	glutathione
GSSG	glutathione disulfide
LA	left atrial
LVIDd	left ventricular internal diameter at end-diastole
LVIDs	left ventricular internal diameter at end-systole
MAPK	mitogen-activated protein kinase
MCU	mitochondrial calcium unidirectional transporter
mPTP	mitochondrial permeability transition pore
oxi-CaMKII	oxidation of calcium/calmodulin-dependent protein kinase II
ROS	reactive oxygen species
SR	sarcoplasmic reticulum

simply a "garbage" product of APP metabolism; it is a peptide that can activate the α7nAChR and release neurotransmitters to enhance synaptic plasticity through a significant increase of Ca^{2+} [14,15]. Additionally, α7nAChR has been described in various non-neuronal cell types, including cardiac fibroblasts and cardiomyocytes [16,17]. Recent study has showed activation of α7nAChR by lipoprotein(a) induced cardiomyocyte apoptosis and inflammation via CaMKII/ERK/p38 MAPK pathways, which could be suppressed by garcinol [18]. However, whether Aβ can affect α7nAChR in cardiomyocytes remains unreported and the effect of Aβ-α7nAChR on AF is still unclear.

Oxidative stress may play a key role in Aβ-induced cytotoxicity [19] and is also an often-overlooked aspect of AF pathophysiology on increasing production of reactive oxygen species (ROS) [20]. Impaired intracellular Ca^{2+} handling is a major contributor to promote the activity of CaMKII (calcium/calmodulin-dependent protein kinase II) which promotes atrial remodeling in structure and electrical substrates [21]. It was reported that ROS-dependent CaMKII oxidization is considered as the fundamental mechanism of angiotensin II (Ang II)-induced cardiac dysfunction and arrhythmias [22]. Despite these promising results, the role of CaMKII in atrial alterations impacted by Aβ-α7nAChR has not been tested.

Based on the findings above, we hypothesized that the linking of Aβ and α7nAChR in cardiomyocytes may perform a worsening effect on AF development by CaMKII-dependent mitochondrial oxidative stress damage. Our present study demonstrated that inhibition of α7nAChR reversed Aβ-induced atrial arrhythmogenic remodeling by suppressing mitochondrial oxidative stress via regulation of oxidation of CaMKII (oxi-CaMKII)/MAPK/AP-1 signaling. The present study was designed to reveal underlying mechanisms in the relationship between AD and AF, and found a novel potential therapeutic strategy for AD patients with atrial fibrillation.

2. Methods

2.1. Cell culture and drug treatment

HL-1 cells, mouse atria-derived cardiomyocytes, are similar to primary cardiomyocytes in mitochondrial bioenergetics, metabolism and morphology as an in vitro model [23]. HL-1 cells were purchased from American Type Culture Collection (CRL-1446, ATCC, Shanghai, China). HL-1 cells were cultured in Dulbecco's Modified Eagle Media (DMEM) with 10% FBS (Gibco, California, USA) at 37 °C in a humidified atmosphere of 5% CO_2. The medium was changed every 2 days and cells were sub-cultured once reached 70–80% confluence.

To contribute Aβ-treatment model in vitro, we employed lyophilized amyloid-β 1–42 (HY–P1388, purity = 96.46%, MedChem Express, USA) were dissolved in 1,1,1,3,3,3-hexafluoro-2-propanol (HFIP) to 1 mM to completely monomerized. Re-dissolved the lyophilized amyloid-β in DMSO and diluted it to 1 mM in deionized water. After incubating at 4 °C for 48 h to form oligomers, amyloid-β was diluted in culture media to the final concentration of 50 μM [24]. Then, HL-1 cells were administrated by Aβ after serum starvation, and cells in control group were treated with same volume of DMSO at 0.1% (v/v) in deionized water. α-Bungarotoxin (α-BTX, HY-P1264, MedChem Express, USA), an antagonist of α7nAChR, was chosen to suppress the expression of α7nAChR. α-BTX was dissolved in deionized water to 100 nM. As for over-oxidization model in vitro, we chose Ang II (A9525, Sigma-Aldrich, USA) to administrate HL-1 cells at 1 μM dissolved in DMSO, and control cells were treated with DMSO at 0.1% (v/v). For p38 or ERK inhibition, SB203580 (20 μM, HY-10256, MedChem Express, USA) or PD98059 (25 μM, HY-12028, MedChem Express, USA) were introduced to cell cultures for 2h after Ang II treatment.

2.2. Cell transfection

Short interfering RNA (siRNA) for CaMKII or CaMKII overexpression plasmids based on pCDNA3.1 were constructed and purchased from Hanbio, as well the negative controls. Transfections of HL-1 cells were performed using Lipofectamine 3000 transfection kit (2209761, Invitrogen, USA) according to the manufacturer's protocol.

2.3. Cell viability assay

The viability of HL-1 cells was examined using a Cell Counting Kit (CCK-8, KGA317s, KeyGEN Biotech, Nanjing, China). Briefly, cells were seeded into 96-well plates with a cell density of 5×10^3 cells/well and applied with different treatments. Then, added 10 μL of CCK-8 reagent per well and incubated at 37 °C for 2 h. Optical density (OD) value of each well at 450 nm was detected by a microplate reader (Multiskan FC, Thermo Fisher Scientific Inc., Waltham, MA, USA).

2.4. Apoptosis assay

Apoptosis in vitro was detected using PE Annexin V Apoptosis Detection Kit I (559763, BD Biosciences, USA) according to the manufacturer's instructions. Briefly, HL-1 cells after different treatment were trypsinized at 1×10^6 cells/pipe and washed twice with cold buffer. HL-1 cells were incubated with 5 μl PE-Annexin V and 5 μl 7-AAD for 15 min at room temperature in the dark and measured by BD FACSCelesta flow cytometer. The data were analyzed by Flowjo Software (BD Biosciences, USA).

Apoptosis of atrial tissues was analyzed using TUNEL assay kit (C1086, Beyotime Biotech, Shanghai, China). Sections of atrial tissues were stained with TUNEL assay kit and imaged under a laser-scanning confocal microscope (C2 plus, Nikon, Tokyo, Japan). The images of TUNEL positive for quantification were analyzed using Image J software

(NIH, Baltimore, MD, USA).

2.5. Detection of oxidative stress markers and reactive oxygen species (ROS)

ROS generation in HL-1 cells were determined with dihydroethidium (DHE) assay kit (S0063, Beyotime Biotech, Shanghai, China). The cells were incubated with 5 μl DHE at 37 °C for 15 min in the dark and imaged under a laser-scanning confocal microscope. The levels of GSH/GSSG (S0053) and NAD^+/NADH (S0175) were measured by spectrophotometry using assay kits according to the manufacturer's instructions (Beyotime, China, Shanghai, China). For mitochondrial ROS level in vivo, atrial sections were stained with MitoSOX Red mitochondrial superoxide indicator (5 μM, M36008, Invitrogen, USA) for 15 min at room temperature as described previously [25].

2.6. Analysis of cellular mitochondrial membrane potential, mitochondrial morphology, ATP level and mitochondrial permeability transition pore (mPTP) opening

Mitochondrial membrane potential was measured by JC-1 assay kit (C2003S, Beyotime Biotech, Shanghai, China). HL-1 cells were incubated with JC-1 reagent reagent for 15 min and assessed the JC-1 signals presented as the red to green fluorescence intensity ratio of the dye under a confocal microscope. Mitochondrial morphology and ATP levels was evaluated by Mito-Tracker Red CMXRos (C1049B, Beyotime Biotech, Shanghai, China) and ATP-Red live cell dye (SCT045, Sigma-Aldrich, USA). Mitochondrial permeability transition pore (mPTP) was assessed by mPTP Assay Kit (C2009S, Beyotime Biotech, Shanghai, China) according to the manufacturer's protocol. Briefly, since the mPTP of mitochondria is closed under normal circumstances, $CoCl_2$ cannot enter the mitochondria at this time, after Calcein AM staining and $CoCl_2$ treatment, only the green fluorescence of Calcein will appear in the mitochondria measured using a fluorescence confocal microscope. The images for quantification were analyzed using Image J software.

2.7. Measurement of intracellular and mitochondrial calcium levels

Intracellular Calcium Levels was detected using calcium-sensitive indicator Fluo-3 AM (Thermo Fisher Scientific, Waltham, MA, USA) according to the manufacturer's instructions by BD FACSCelesta flow cytometer. The effect of Aβ-α7nAChR on sarcoplasmic reticulum (SR) calcium kinetics was investigated in Fluo-4(S1060, Beyotime Biotech, Shanghai, China) loaded (5 μmol/L, 30 min, 37 °C) from changes in fluorescence throughout time with respect to the initial value (F/F0, Ex:488 nm/Em:520 nm) after induced by isoproterenol (4 μmol/L) in each group. The mitochondrial calcium levels were measured using Rhod-2 AM (Thermo Fisher Scientific, Waltham, MA, USA). Briefly, HL-1 cells were incubated with 5 μmol/L Rhod-2 AM and 0.02% Pluronic F-127 for 30 min at room temperature. After complete de-esterification of the mitochondrial AM esters, the fluorescence intensities were assessed using a fluorescence confocal microscope. The images for quantification were analyzed using Image J software.

2.8. Animal and drug administration

12-month-old male wild-type C57BL/6J mice (WT) and age-matched overexpressing hAPP695swe and presenilin-1 transgenic mice (APP/PS1) were purchased from Beijing HFK bioscience co., LTD (Beijing, China). All animal-related procedures were approved by the General Hospital of Northern Theatre Command Animal Care Committee and conducted in strict compliance with Institutional Animal Care and Use protocols. All mice were group-housed (3–4 mice/cage) at room temperature (24 ± 2 °C) exposed to a 12h/12h light-dark cycle with free access to water and food.

2.9. Adeno-associated virus (AAV) transfection in vivo

To evaluated the effect of α7nAChR on WT or APP/PS1 mice, an adeno-associated virus (AAV) 2/9 containing Chrna7-specific small hairpin RNA (AAV-Chrna7) or scrambled shRNA (AAV-CON) with cardiac troponin T (cTnT)-promoter (viral titer = 2×10^{12}vg/ml) were structured by HanBio. 12-month-old mice were injected 100 μl AAV through the caudal veins to establish a cardiomyocyte-specific α7nAChR gene knockout model. Follow up tests were carried out after 28 days of injection.

2.10. Hemodynamic parameters

Hemodynamic parameters, including heart rate (HR), systolic and diastolic blood pressure were noninvasively evaluated by a pressure recording sensor and the tail cuff (BP-2010A, Softron Beijing Biotechnology Co., Ltd, Beijing, China). Mice were tested on day 28 after AAV injection.

2.11. Mouse echocardiography

Echocardiography was performed as reported previously [26]. Briefly, transthoracic echocardiography (D700, Vinno Technology Co., Ltd, Suzhou, China) was performed, as mice were anesthetized with 1.5% isoflurane. Left atrial diameter (LAD), LA systolic area, LA diastolic area, left ventricular internal diameter at end-diastole (LVIDd), left ventricular internal diameter at end-systole (LVIDs) and ejection fraction (EF) were determined in the parasternal long axis view from M-mode images recorded over at least three cardiac cycles.

2.12. Mouse ECG recording and AF induction

The mice were anesthetized with isoflurane (2.0%) (VME, Matrx, USA) and fixed on the console. A surface 3-lead echocardiogram (ECG) was recorded (FE132-0641, ADinstruments Co Ltd., New South Wales, Australia) and analyzed with LabChart 8 (ADinstruments Co Ltd., New South Wales, Australia). We pricked a tiny hole on the right cervical vein of each mouse for performing an electrode catheter (FTS-1113A-1018, Transonic scisense Inc., Ontario, Canada) into atria. All mice underwent burst pacing by physiological signal acquisition and analysis system (RA834, iWorx, USA) with amplitude of 6V, cycle length of 40 ms, pulse duration of 6 ms, and stimulation time of 30s. Repeated the stimulation for 5 times and recorded the AF incidence and duration. AF incidence was defined as rapid, irregular atrial response over 2 s. AF duration was defined as the time from AF initiation to SR turning back.

2.13. Langendorff-perfused isolated hearts and electrical mapping of ex vivo heart preparations and arrhythmia induction

The mice were sacrificed by intraperitoneal injection with sodium pentobarbital (5 mg/100g). Hearts were rapidly excised by thoracotomy and mounted onto a Langendorff perfusion system perfused with Tyrode's solution (140 mM NaCl, 5 mM KCl, 1 mM $MgCl_2$, 5 mM HEPES, 10 mM D-glucose, 1.8 mM $CaCl_2$, PH = 7.3–7.4, and equilibrated with 5% CO_2 and 95% O_2) with the flow rate of 8 ml/min at 37 °C. Hearts were stabilized with perfusion for 10 min before experimental procedures commenced. To activate and antagonize α7nAChR, we successively perfused hearts with nicotine (100 μM) and α-BTX (100 μM) and the procedure was shown in Fig. 6D.

A multi-electrical array (MEA) mapping system (EMS128, MappingLab Ltd., Oxford, UK) was employed to record extracellular potentials (ECP). A 64 channel MEAs (MappingLab Ltd., Oxford, UK) were employed for left atrial simultaneous recordings. ECP signals were recorded using EMapRecord 5.0 software (MapingLab Ltd., Oxford, UK). The cardiac isochronal activation map was plotted as time differences between the first activation site and the individual activation site on

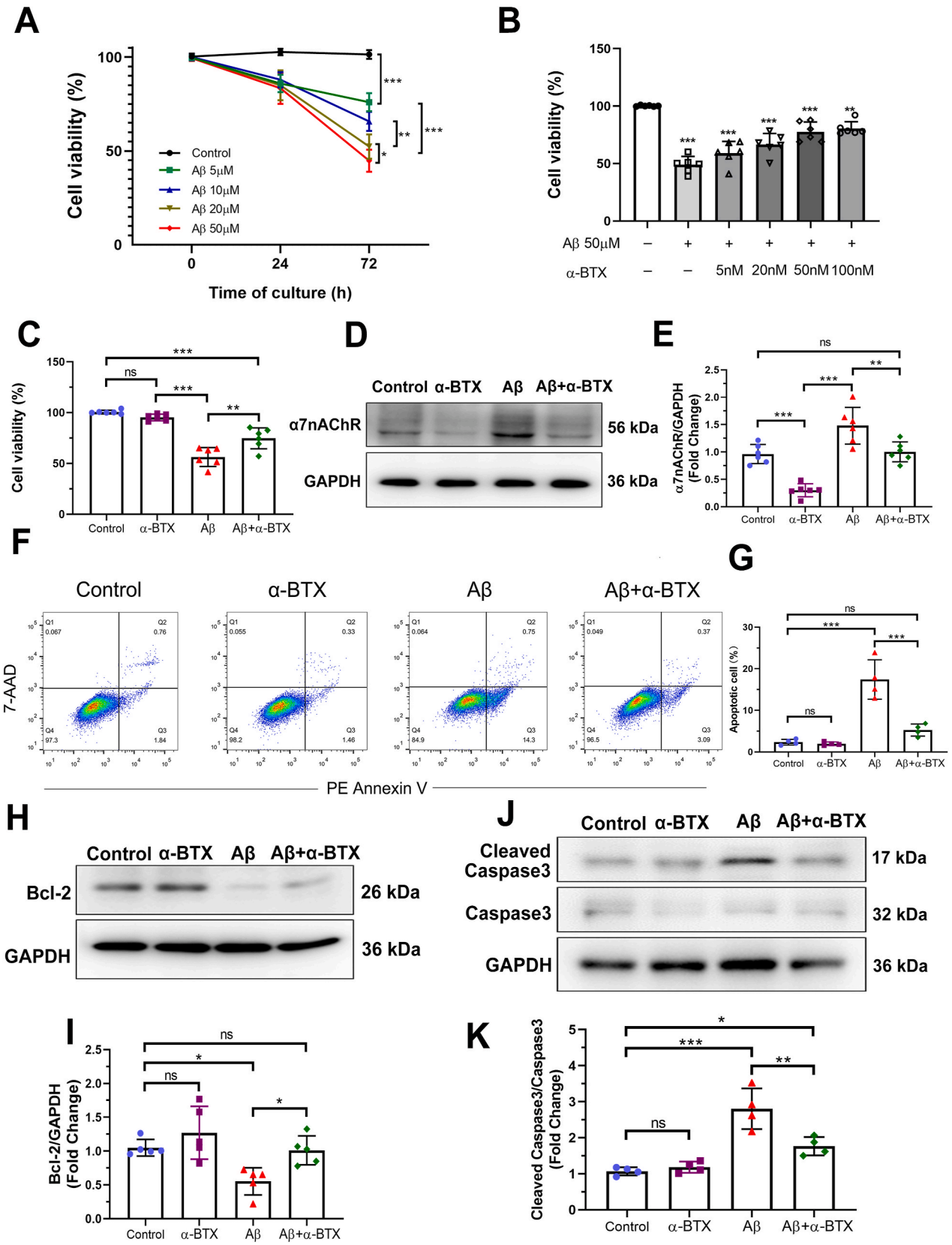

Fig. 1. α-BTX prevented Aβ long-term induced cytotoxicity and apoptosis in HL-1 cells in vitro. HL-1 cells were treated with (A) Aβ (0, 5, 10, 20 and 50 μM) for 24 and 72 h, or (B) α-BTX (0, 5, 20 and 50 nM) followed by Aβ (50 μM) for 72h. CCK-8 assays were performed to measure cell viability (n = 6). (C) 50 μM Aβ and/or 50 nM α-BTX administration of HL-1 cells at 72 h were selected for subsequent experiments using CCK-8 assay (n = 6). (D, E) α7nAChR protein level in HL-1 cells treated by 50 μM Aβ and/or 50 nM α-BTX, which were quantified in each group (n = 6). (F–G) Apoptosis was evaluated by flow cytometry using PE Annexin-V/7-AAD staining (n = 4). (H–K) Representative western blotting and quantitative analysis of Bcl-2, Cleaved Caspase3 and Caspase3 (n = 5). Data were presented as Mean ± S.D. $^{ns}P > 0.05$, $^{*}P < 0.05$; $^{**}P < 0.01$ and $^{***}P < 0.001$.

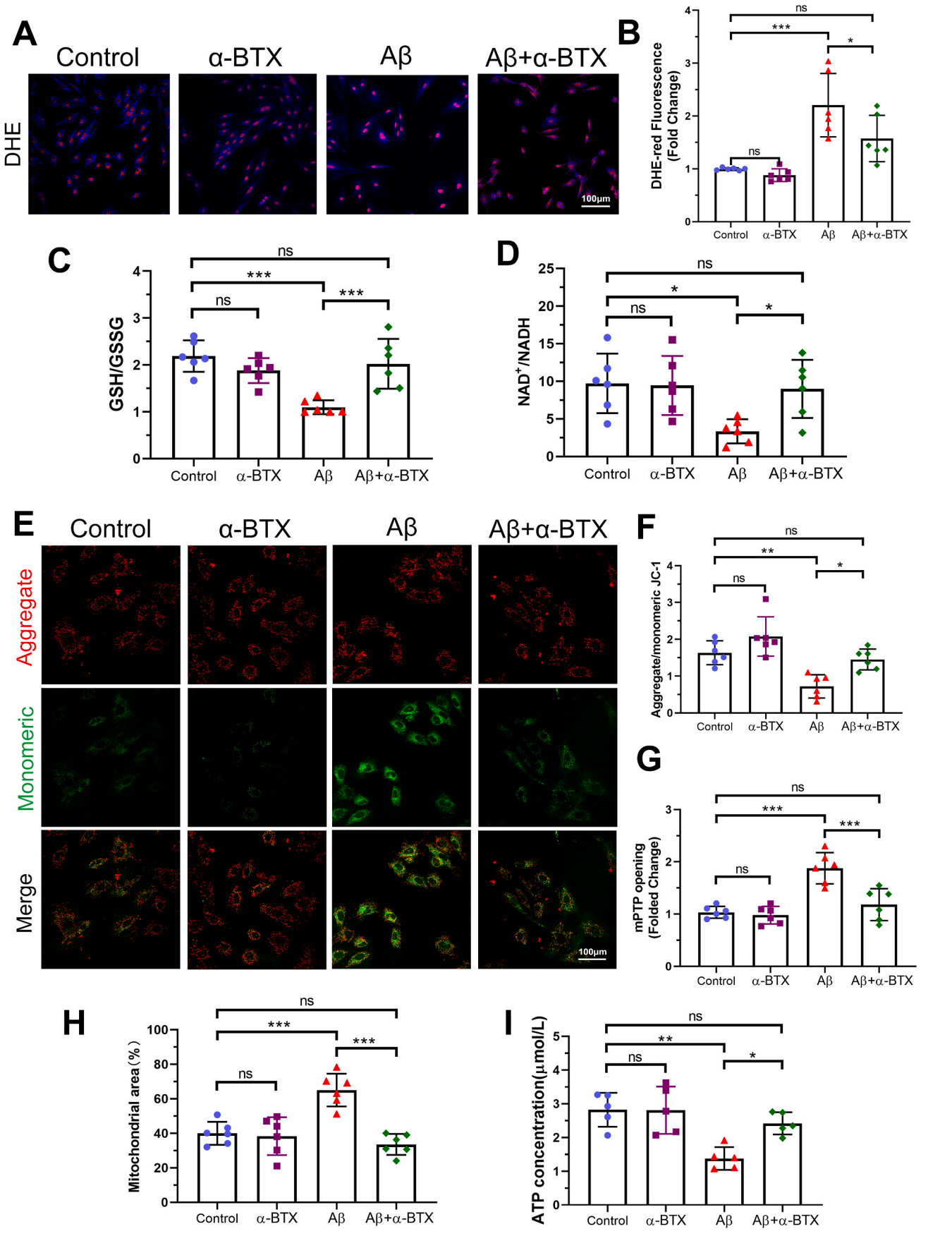

(caption on next page)

Fig. 2. α-BTX attenuated Aβ-induced oxidative stress and mitochondrial dysfunction in vitro. (A, B) Representative images and quantitative analysis showing the levels of reactive oxygen species (ROS) of each group as measured by DHE staining (red). (C) Quantifications of glutathione (GSH)/glutathione disulfide (GSSG) ratio. (D) Quantifications of NAD^+/NADH. (E, F) Representative images of aggregate (red)/monomeric (green) JC-1 fluorescence and quantitative analysis in HL-1 cells from each group. (G) Quantifications of mPTP opening evaluated using fluorescence intensity after treatment of Calcein AM and $CoCl_2$. (H) Quantifications of mPTP opening evaluated using Mito-Tracker. (I) Quantifications of ATP concentration. n = 6 per group in each independent experiment. Data were presented as Mean ± S. D. $^{ns}P > 0.05$, $^{*}P < 0.05$, $^{**}P < 0.01$ and $^{***}P < 0.001$. Calibration bar = 100 μm. (For interpretation of the references to color in this figure legend, the reader is referred to the Web version of this article.)

each channel. Activation times were calculated as the point of maximal negative slope of activation waveforms. The atrial conduction velocity was calculated from the conduction timing and the known distance between the recording points. The inhomogeneity index was calculated though the activation sequence. All mapping data were analyzed using EMapScope 5.0 software (MappingLab Ltd., Oxford, UK).

2.14. Histopathological analysis

Atrial tissues were fixed in 4% paraformaldehyde for Masson's trichrome staining. Tissues were paraffin-embedded and cut into 5 μm sections. Masson's trichrome staining assay (KGMST-8004, KeyGEN Biotech, Nanjing, China) was used to evaluate the fibrosis. Additionally, the fibrotic areas were analyzed using Image J software. The percentage of fibrosis is shown as the ratio of blue-stained area normalized to the total area.

The sections were used for immunofluorescent staining as described previously [27]. Brifly, the cell samples or sections were incubated for 1h in 5% BSA and 0.3% Triton X-100. Then they were incubated with anti-Nicotinic acetylcholine receptor α7 (ab216485, Abcam, Cambridge, MA, USA) and anti-CaMKII (ab134041, Abcam, Cambridge, MA, USA) overnight at 4 °C. Next, rinsed thrice with PBS and incubated with fluorescent second antibody antibodies for 1h. After washing with PBS twice, the samples were counterstained with DAPI (C1002, Beyotime Biotech, Shanghai, China) for nucleus visualizing, and photographed using a fluorescent confocal microscope. The images for quantification were analyzed using Image J software.

For investigating the location of CaMKII, immunofluorescence assay using both Mito-Tracker Red CMXRos (C1049B, Beyotime Biotech, Shanghai, China) and anti-CaMKII (ab134041, Abcam, Cambridge, MA, USA) was performed and the following steps were described above. The colocation of CaMKII and Mito-Tracker visualized by yellow staining were analyzed using Image J software.

2.15. Total collagen assay

The collagen was evaluated by the total collagen assay kit (ab222942, Abcam, Cambridge, MA, USA). The assay is based on the Alkaline hydrolysis of atrial tissues to release hydroxyproline combined oxidized to brightly-colored chromophore, which can be easily detected at OD 560 nm by microplate reader (Multiskan FC, Thermo Fisher Scientific Inc., Waltham, MA, USA). The manipulation was performed in strict accordance with the manufacturer's instructions. The protein contents were quantified against a standard curve calibrated with known amounts of protein. Samples were assayed in triplicate.

2.16. Inflammatory factor detection

The levels of tumor necrosis factor (TNF) -α (PT512), interleukin (IL) -1β (PI522), IL-6 (PI326) and IL-10 (PI522) in atria were tested via enzyme-linked immunosorbent assay (ELISA) using mouse ELISA kit, which were purchased from Beyotime Biotech, and the tests were performed according to the manufacturer's instructions.

2.17. Western blotting

The Western blotting assays were performed according to the previous description [26]. Briefly, HL-1 cells or atrial tissues were lysed with Radio Immunoprecipitation Assay (RIPA) lysate containing 1 mM phenylmethyl sulfonyl fluoride (PMSF). The samples were lysed on ice for 30 min and centrifuged at 12,000 rpm for 30 min. Afterwards protein concentration was determined by BCA method (P0012, Beyotime Biotech, China), the protein concentration was adjusted and placed in 100 °C boiling water for 7 min. Use sodium dodecyl sulfate-polyacrylamide (SDS-PAGE) gel electrophoresis, electro-transfer method to transfer the protein to polyvinylidene (PVDF) membrane (IPVH00010, Millipore Corporation, Billerica, MA, USA). The primary antibody at 4 °C overnight, including α7nAChR (ab216485, Abcam, USA), Bcl-2 (sc-7382, Santa Cruz, USA), Cleaved Caspase3 (9661s, CST, USA), Caspase3 (93815s, CST, USA), NCX1 (ab177952, Abcam, USA), Serca2 (ab150435, Abcam, USA), RYR2 (A0298, ABclonal, China), CaMKII (ab134041, Abcam, USA), mitochondrial calcium unidirectional transporter (MCU) (14997, CST, USA), oxi-CaMKII (GeneTex, gtx36254, USA), p-p38 (4511, CST, USA), p38 (8690s, CST, USA), p-Erk (8544s, CST, USA) and Erk (4695s, CST, USA), c-Fos (2250t, CST, USA), c-Jun (9165s, CST, USA), GAPDH (5174s, CST, USA) and β-actin (AF5001, Beyotime, China). Incubated in the goat anti-rabbit IgG (A0208, Beyotime, China) or goat anti-mouse IgG (A0216, Beyotime, China) secondary antibodies for 1h at room temperature. The protein expression was detected by chemiluminescence HRP substrate (WBKLS0500, Millipore, USA) with electrochemiluminescence (ECL) derive (Tanon-5200, bioTanon, Shanghai, China). The optical density of each band was measured using Quantity One software (Bio-Rad, USA).

2.18. Statistical analyses

Continuous data are expressed as Mean ± S.D. deviation and categorical data were expressed as percentages. Student's t-test were performed to comparing two groups. One-way ANOVA followed by the Turkey's comparison test was used to assess the differences among multiple groups. The statistical analysis is completed with SPSS 22.0 software (IBM, Chicago, IL, USA). The statistical significance was defined as $P < 0.05$.

3. Results

3.1. α-BTX prevented Aβ long-term induced cardiomyocyte death in vitro

Aβ has been reported to induce cardiomyocyte death. To investigate the exact effect of α7nAChR on Aβ-induced cytotoxicity, cell viability assays were determined in HL-1 cells. Within 24 h, Aβ treatment at 5 μm up to 50 μM did not show any significant differences in cell viability. Cytotoxicity effects of Aβ at 20 μM and 50 μM were markedly increased after 72 h treatment (Fig. 1A), indicating a long-term regulation of Aβ on HL-1 cells. α-BTX dose-dependently reversing cytotoxicity effects of Aβ were detectable as well (Fig. 1B). Thus, 50 μM Aβ and 50 nM α-BTX at 72 h administration were chosen in subsequent experiments (Fig. 1C). Furthermore, we investigated the effects of α-BTX on α7nAChR expression against Aβ treatment on HL-1 cells. Compared to the control group, HL-1 cells treated by Aβ at 50 μM for 72 h showed dramatically increased level of α7nAChR, which could be down-regulated by α-BTX (Fig. 1D and E). Apoptosis analysis using flow cytometry of staining with Annexin V/7-AAD revealed that apoptotic cells in Aβ group was significantly more than those in Control, α-BTX and Aβ+α-BTX groups, respectively (Fig. 1F and G). Aβ treatment significantly promoted the Cleaved Caspase3, a pro-apoptotic protein, and reduced Bcl-2, an anti-

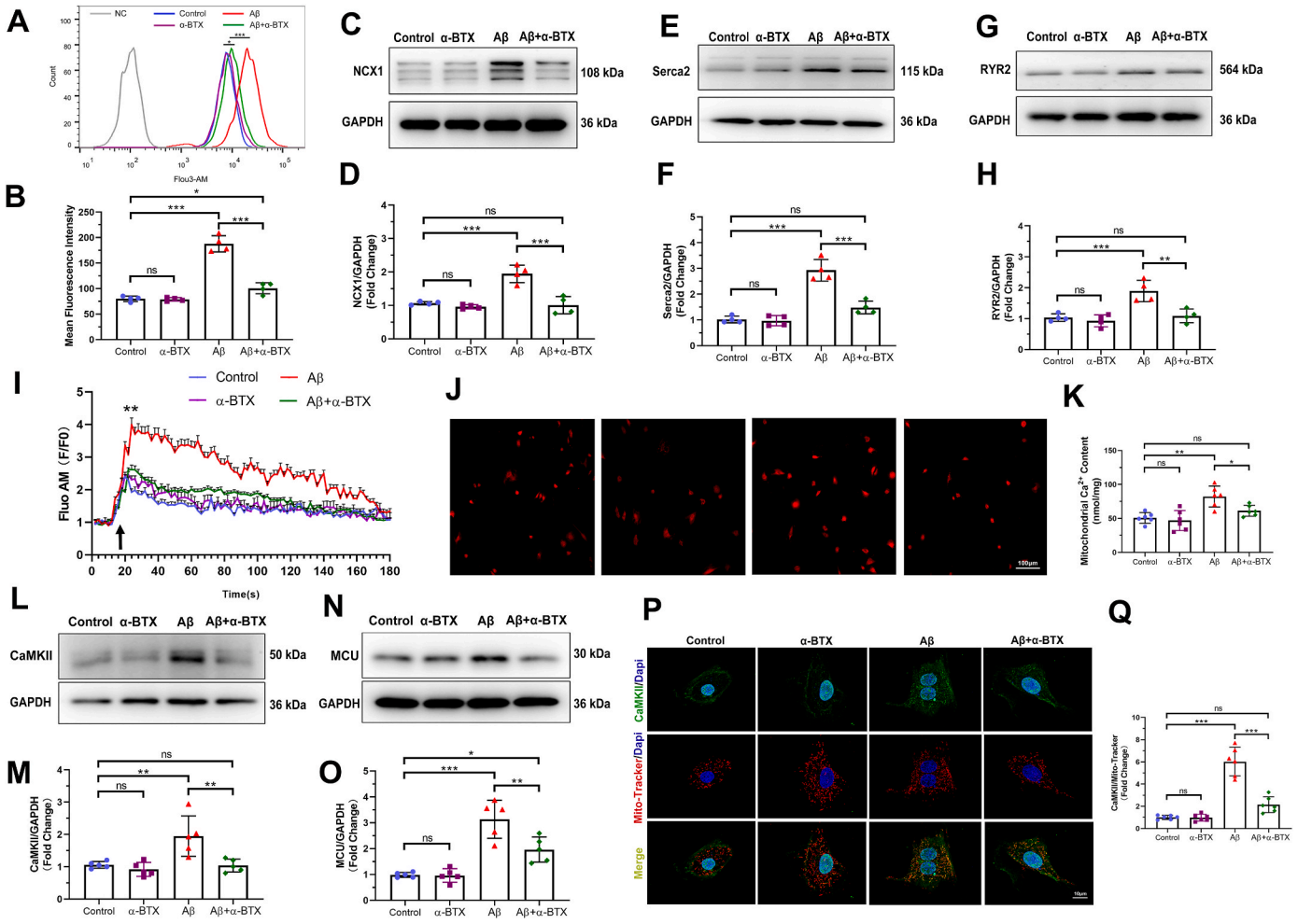

Fig. 3. α-BTX restrained Aβ-induced Ca^{2+} mishandling and CaMKII expression of mitochondria in vitro. (A, B) Intracellular Ca^{2+} levels were evaluated by flow cytometry using Fluo 3-AM calcium indicator and quantified in HL-1 cells of each group (n = 4). (C, D) Representative western blotting and quantitative analysis of NCX1 (n = 4). (E, F) Representative western blotting and quantitative analysis of Serca2 (n = 4). (G, H) Representative western blotting and quantitative analysis of RYR2 (n = 4). (I) Kinetics of calcium uptake (Fluo AM F/F0) with isoproterenol (black arrow) in HL-1 cells of each group (n = 6), $^{**}P < 0.01$ compare with Control group. (J, K) Representative images and quantifications of mitochondrial Ca^{2+} content (n = 6). Calibration bar = 100 μm. (L, M) Representative western blotting and quantitative analysis of CaMKII (n = 5). (N, O) Representative western blotting and quantitative analysis of MCU (n = 5). (P, Q) Representative images and quantitative analysis of colocalization of CaMKII (green) and Mito-Tracker (red) fluorescence in HL-1 cells of each group (n = 6). Calibration bar = 10 μm. Data were presented as Mean ± S.D. $^{ns}P > 0.05$, $^{*}P < 0.05$, $^{**}P < 0.01$ and $^{***}P < 0.001$. (For interpretation of the references to color in this figure legend, the reader is referred to the Web version of this article.)

apoptotic protein, while α-BTX significantly reversed these changes (Fig. 1H–K). These results indicate that α-BTX prevents Aβ-induced cytotoxicity and apoptosis through α7nAChR in vitro.

3.2. *α7nAChR inhibiting by α-BTX attenuated Aβ-induced oxidative stress and mitochondrial dysfunction in vitro*

Previous studies have shown that Aβ-induced cytotoxicity is closely related to oxidative stress damage and mitochondrial dysfunction [28]. Therefore, we investigated the role of mitochondria function in HL-1 cells exposed to Aβ and/or α-BTX. Aβ treatment induced oxidative stress damage as evidenced by increased DHE-red staining and decreased GSH/GSSG and NAD^+/NADH ratio, which were reversed by α-BTX (Fig. 2A–D and Supplementary Figs. 1A–B). Compared with Control, α-BTX and Aβ+α-BTX groups, administration of Aβ markedly induced depolarization of the mitochondrial membrane characterized by decreased ratio of aggregate/monomeric JC-1 and mPTP opening assay (Fig. 2E–G, Supplemental Fig. 1C). Furthermore, α-BTX-treated cells were also protected against Aβ-induced swelling of mitochondria and decreased ATP generation capacity, as evidenced by a decreased mitochondrial area and increased ATP concentration, compared with those in the Aβ group (Fig. 2H and I, Supplementary Fig. 1D). These data suggested that α-BTX inhibited Aβ-induced oxidative stress and mitochondrial dysfunction in HL-1 cells. Interestingly, there were no dramatically differences between control and α-BTX groups in all above tests, indicating that the inhibitory effects of α-BTX on oxidative stress and mitochondrial dysfunction were only with regard to Aβ.

3.3. *α-BTX restrained Aβ-induced Ca^{2+} mishandling and CaMKII expression of mitochondria in vitro*

Given the high permeability of α7nAChR to Ca^{2+}, we investigated the intracellular Ca^{2+} level using Fluo 3-AM calcium indicator to administrate HL-1 cells. The mean fluorescence intensity (MFI) of Aβ group was significantly increased comparing with those of Control, α-BTX and Aβ+α-BTX groups (Fig. 3A and B). Considering the importance of sarcoplasmic reticulum in Ca^{2+} balance in the cytosol, we investigated the Ca^{2+} handling proteins level and Ca^{2+} kinetics in four groups. Western blotting analysis demonstrated increased expression levels of NCX1, Serca2 and RYR2 in Aβ group compared with the other three

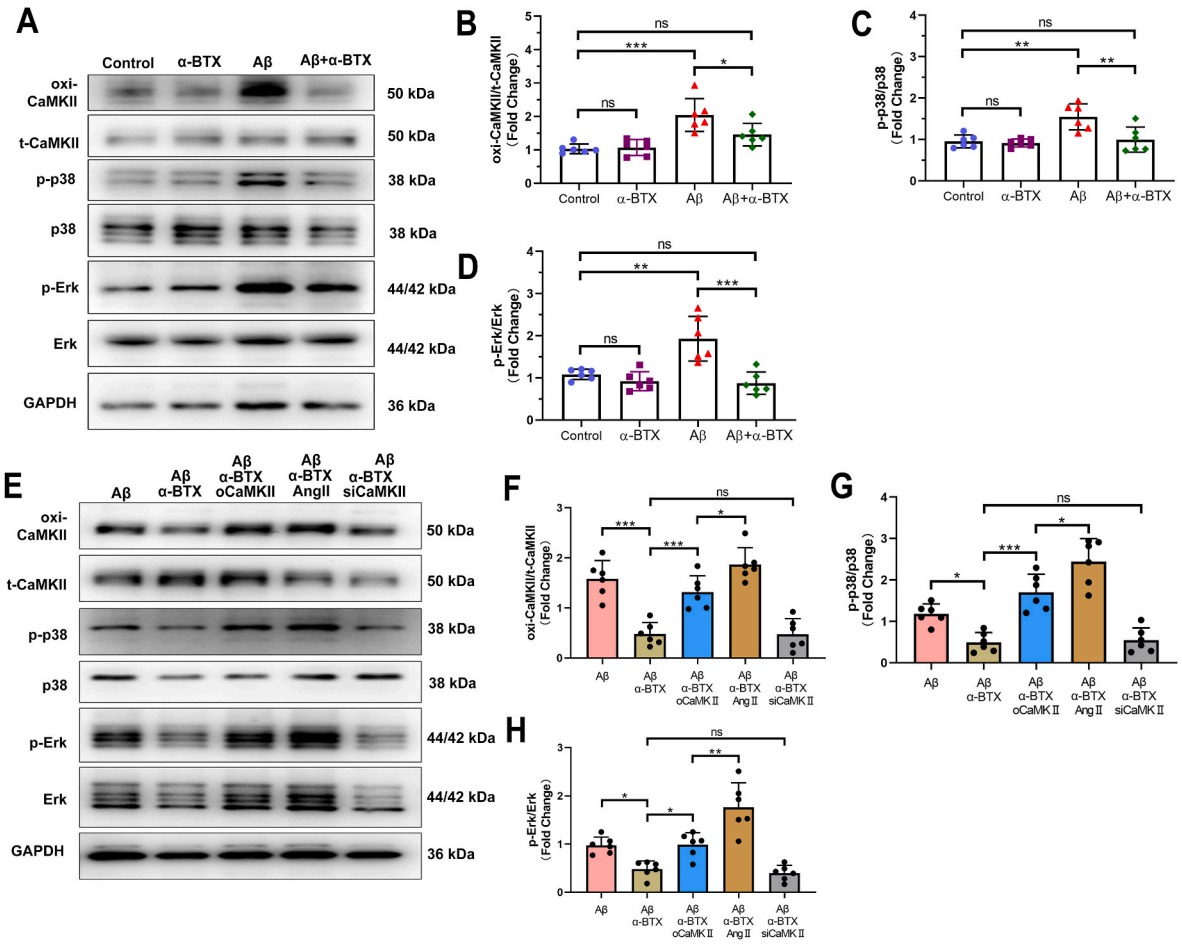

Fig. 4. The protective effects of α-BTX against Aβ-prompted MAPK signaling pathway were regulated by CaMKII activity and expression. (A–D) Representative western blotting and quantitative analysis of oxi-CaMKII/t-CaMKII, p-p38/p38 and p-Erk/Erk in HL-1 cells with/without Aβ or α-BTX treatment. (E–H) Representative western blotting and quantitative analysis of oxi-CaMKII/t-CaMKII, p-p38/p38 and p-Erk/Erk in Aβ and α-BTX treated HL-1 cells with overexpression of CaMKII (oCaMKII), angiotensin II (AngII) or knockdown CaMKII (siCaMKII). n = 6 per group in each independent experiment. Data were presented as Mean ± S.D. $^{ns}P > 0.05$, $^{*}P < 0.05$, $^{**}P < 0.01$ and $^{***}P < 0.001$.

groups (Fig. 3C–H). Moreover, Aβ treatment resulted in more efficient Ca^{2+} uptake, which suppressed by α-BTX (Fig. 3I). In order to determine whether Aβ-induced Ca^{2+} uptake in response to sarcoplasmic reticulum calcium release, a mitochondrial Ca^{2+} content assay was followed. We found an increase in Ca^{2+} level in mitochondria of Aβ group, which was restrained by α-BTX treatment (Fig. 3J and K), suggesting a Ca^{2+} overload in mitochondria of Aβ treated cells and an inhibitory effect of α-BTX in it. CaMKII, a critical Ca^{2+} and reactive oxygen species (ROS) sensor, and mitochondrial calcium unidirectional transporter (MCU), the key mitochondrial Ca^{2+} uniporter complex, were thought to influence the mitochondrial Ca^{2+} handling [29,30]. With this in mind, we found a significantly increase in the CaMKII and MCU expression of Aβ treatment and α-BTX markedly decreased Aβ-induced the high level of CaMKII and MCU (Fig. 3L–O). Furthermore, conventional immunofluorescence showed an increased colocalization of CaMKII and Mito-Tracker in Aβ groups compared to the other groups (Fig. 3P and Q), suggesting an accumulation of CaMKII in mitochondria of Aβ treated HL-1 cells. These results indicate that Aβ leads to Ca^{2+} overload and α-BTX can prevent this process via regulating MCU and CaMKII in mitochondria.

3.4. The protective effects of α-BTX against Aβ-prompted MAPK signaling pathway were regulated by oxi-CaMKII activity and expression

To determine the role of α7nAChR in Aβ-mediated mechanism of HL-1 cells in vitro, CaMKII and downstream proteins were investigated. α-BTX significantly suppressed the Aβ-prompted high radio of oxidation of CaMKII (oxi-CaMKII)/total CaMKII (t-CaMKII), indicating the important role of oxi-CaMKII in the effect of Aβ-α7nAChR in HL-1 cells (Fig. 4A and B). We next investigated CaMKII related proteins and found that Aβ markedly increased the p-p38/p38 and p-Erk/Erk, which could be also downregulated by α-BTX (Fig. 4A, C-D).

In order to clarify the involvement of CaMKII in Aβ-α7nAChR mechanism, we set up three additional groups which CaMKII were overexpressed using CaMKII overexpression plasmid (oCaMKII), knockout using siRNA-CaMKII (siCaMKII) or oxidated by AngII treatment in vitro (Supplementary Fig. 2). As shown in Fig. 4E–H, western blotting showed that knockout of CaMKII, siCaMKII group, could not further down regulated the phosphorylation of MAPK key proteins (p38 and Erk) on the basis of α-BTX, which might be due to α-BTX down-regulated CaMKII to reach the threshold, so it could not be further reduced. While treatment with overexpression of CaMKII, oCaMKII group, and AngII significantly activated CaMKII and MAPK pathway. Importantly and notably, the effect of AngII on MAPK pathway became more evident compared to CaMKII overexpression, suggesting that oxi-CaMKII directly promoted by AngII played a more considerable role in mediating Aβ-α7nAChR effect in HL-1 cells.

To determine the roles of Erk and p38 activation in oxi-CaMKII-promoted oxidative stress in vitro, HL-1 cells were treated with p38 inhibitor SB203580 or Erk inhibitor PD98059 (Fig. 5A–C). Both SB203580 and PD98059 removed the AngII-induced increase of

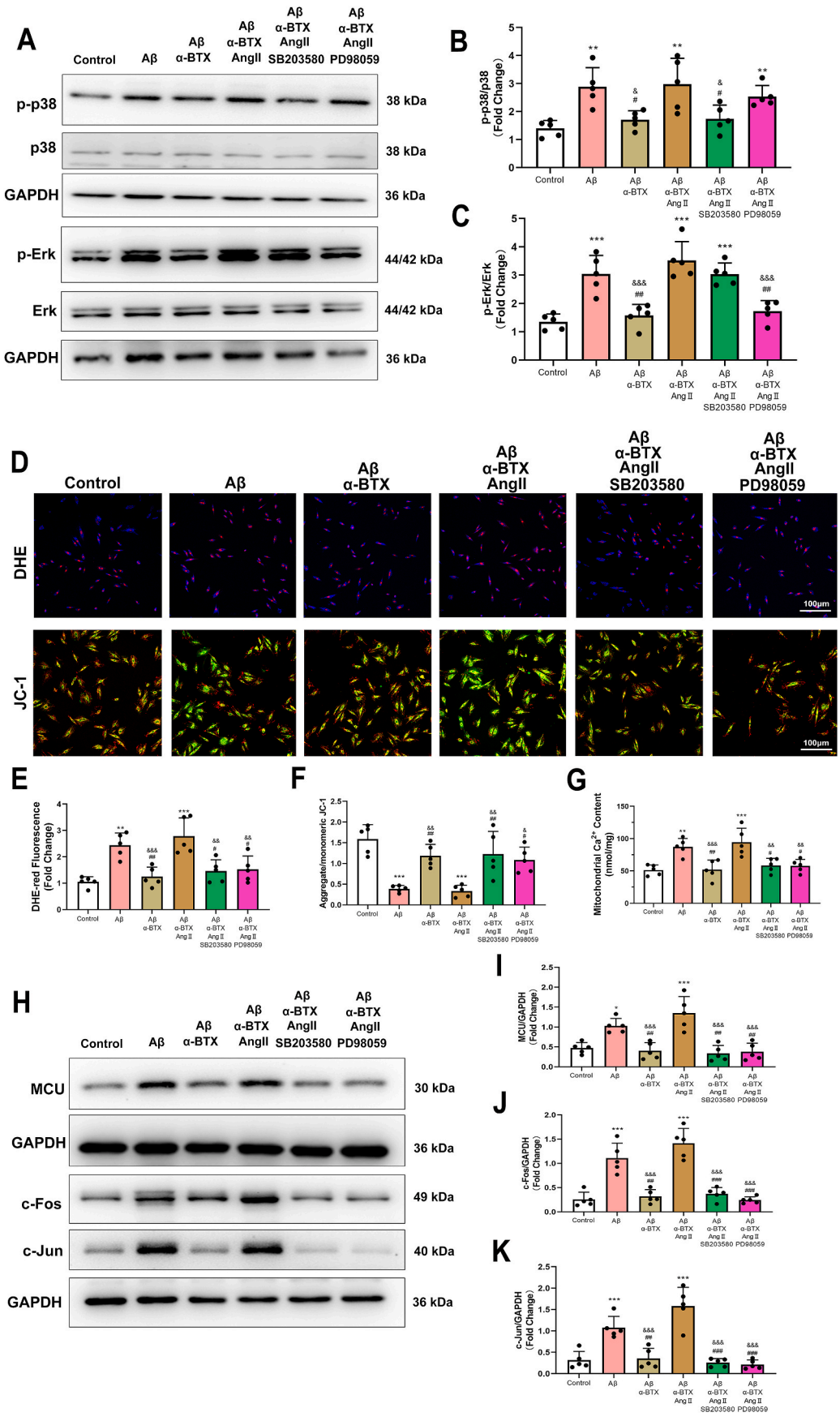

Fig. 5. Inhibition of p38 or Erk reversed Aβ/α7nAChR/oxi-CaMKII induced oxidative stress and mitochondrial dysfunction in vitro. (A–C) Representative western blotting and quantitative analysis of p-p38/p38 and p-Erk/Erk in HL-1 cells with p38 or Erk inhibitor. (D–F) Representative images and quantitative analysis showing DHE staining and JC-1 fluorescence in HL-1 cells of each group. (G) quantifications of mitochondrial Ca^{2+} content. (H–K) Representative western blotting and quantitative analysis of MCU, c-Fos and c-Jun and in HL-1 cells of each group. Calibration bar = 100 μm. Data were presented as Mean ± S.D. $^{*}P < 0.05$, $^{**}P < 0.01$ and $^{***}P < 0.001$, compare to Control group; $^{*}P < 0.05$, $^{**}P < 0.01$ and $^{***}P < 0.001$, compare to Control group; $\#P < 0.05$, $\#\#P < 0.01$ and $\#\#\#P < 0.001$, compare to Aβ group; $\&P < 0.05$, $\&\&P < 0.01$ and $\&\&\&P < 0.001$, compare to Aβ+α-BTX + AngII group.

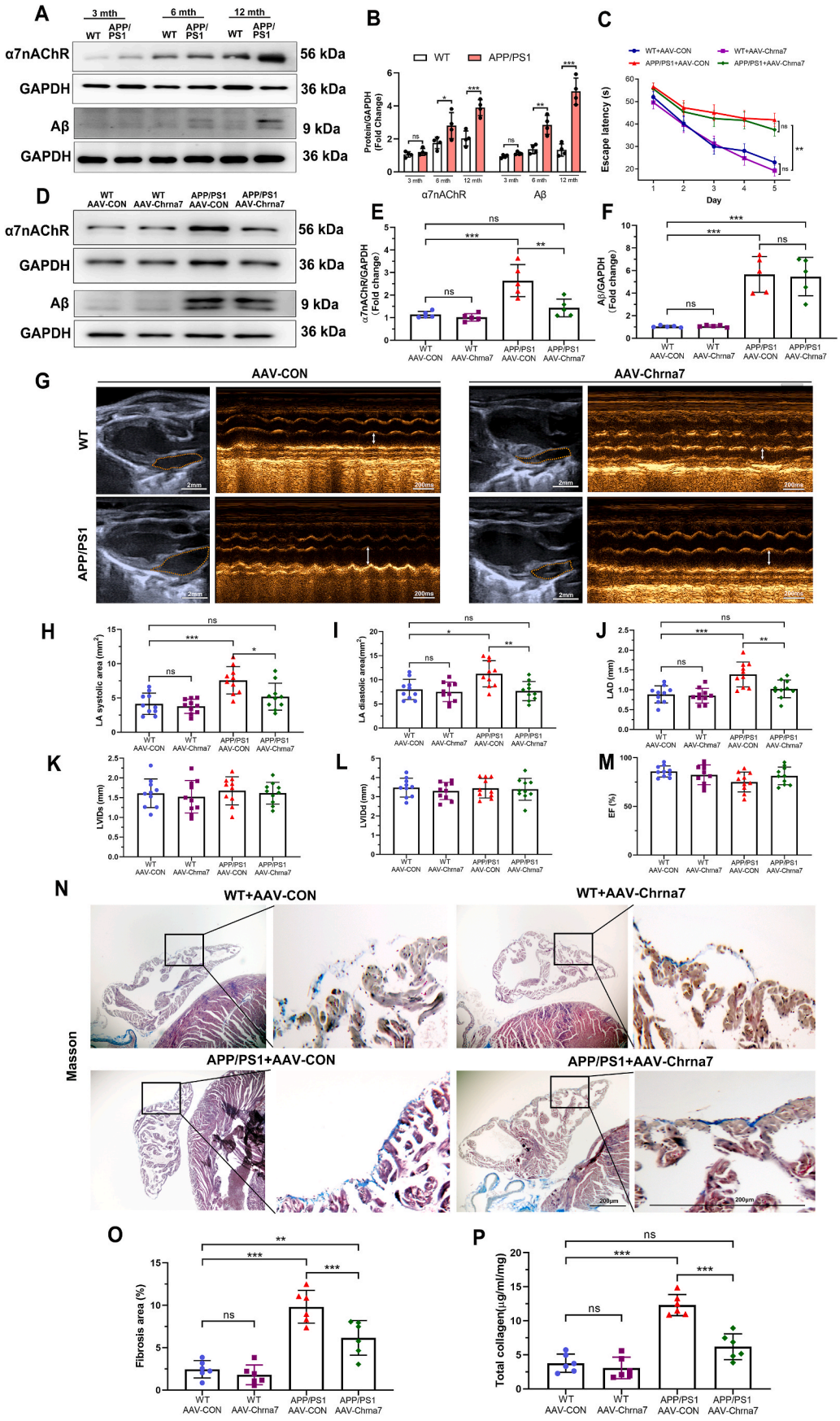

Fig. 6. Silencing α7nAChR in cardiomyocytes attenuated structure remodeling in aged APP/PS1 mice. (A, B) Representative western blotting and quantitative analysis of Aβ and α7nAChR in the atrial tissues of WT and APP/PS1 mice at 3, 6 and 12 months of age (n = 4). (C) Quantitative analysis of escape latency for 12-month-old mice in each group. (D–F) Representative western blotting and quantitative analysis of Aβ and α7nAChR in the atrial tissues of 12-month-old mice in each group (n = 5). (G) Measured echocardiographic positioning (Calibration bar = 2 mm) and the M-mode images (bar = 200 ms) of left atria (LA). Quantitative analysis of (H) LA systolic area, (I) LA diastolic area, (J) left atrial diameter (LAD), (K) left ventricular internal diameter at end-diastole (LVIDd), (L) left ventricular internal diameter at end-systole (LVIDs) and (M) ejection fraction (EF) (n = 10). (N) Representative images of Masson trichrome staining of left atria. Blue staining indicated collagen fibers and red staining indicated muscle fibers (Calibration bar = 200 μm). (O) Quantitative analysis of atrial fibrosis area (n = 6). (P) Quantitative analysis of total atrial collagen (n = 6). Data were presented as Mean ± S.D. $^{ns}P > 0.05$, $^{*}P < 0.05$, $^{**}P < 0.01$ and $^{***}P < 0.001$. (For interpretation of the references to color in this figure legend, the reader is referred to the Web version of this article.)

Table 1
Physiological characteristics
BW, body weight; HW, heart weight; HW/BW, heart weight/body weight; SBP, systolic Blood Pressure; DBP, diastolic Blood Pressure; MBP, mean Blood Pressure; HR, heart rate.

Variables	WT + AAV-CON	WT + AAV-Chrna7	APP/PS1+AAV-CON	APP/PS1+AAV-Chrna7	*F*	*P*
BW, g	26.24 ± 0.75	24.82 ± 1.02	25.65 ± 0.62	25.98 ± 0.66	0.623	0.609
HW, mg	144.95 ± 2.44	142.30 ± 5.63	138.75 ± 1.59	145.18 ± 1.49	3.718	0.049
HW/BW, mg/g	5.55 ± 0.17	5.79 ± 0.35	5.43 ± 0.15	5.61 ± 0.18	0.308	0.740
SBP, mmHg	155.33 ± 5.40	166.50 ± 4.47	162.17 ± 2.52	157.17 ± 2.90	1.593	0.222
DBP, mmHg	64.50 ± 2.97	66.17 ± 4.48	62.83 ± 2.27	64.33 ± 6.25	0.470	0.707
MBP, mmHg	91.00 ± 3.08	87.00 ± 4.40	92.67 ± 2.92	93.33 ± 2.09	0.774	0.522
HR, bpm	585.33 ± 10.12	544.80 ± 18.20	592.83 ± 7.28	580.33 ± 10.56	3.033	0.053

oxidative stress and mitochondrial damage as evidenced by increased DHE-red staining and decreased ratio of aggregate/monomeric JC-1 (Fig. 5D–F), indicating that oxi-CaMKII upregulation induced by AngII promoted oxidative stress and mitochondrial damage, which was p38 and Erk dependent. Interestingly, SB203580 and PD98059 treatment reverse the AngII-induced mitochondrial Ca^{2+} overload (Fig. 5G) and MCU expression (Fig. 5H and I), suggesting p38 and Erk could regulate the mitochondrial Ca^{2+} by mediating MCU function. (Fig. 5H and I). Notably, AngII-induced up-regulation of transcription factor, c-Jun and c-Fos, was diminished by SB203580 and PD98059 (Fig. 5H,J,K).

3.5. Silencing α7nAChR in cardiomyocytes attenuated structure remodeling in aged APP/PS1 mice

In order to confirm the role of Aβ-α7nAChR in atrial dysfunction, APP/PS1 mice were utilized to confirm the effect of Aβ on atrial remodeling. First, we investigated expression of Aβ and α7nAChR in the atria of WT and APP/PS1 mice in 3, 6 and 12 months old. As mice aged, the expression of α7nAChR in WT and APP/PS1 mice were gradually increased. Compared to WT mice at 12 months old, α7nAChR and Aβ expression levels of APP/PS1 mice were significantly increased, indicating that the effect of Aβ deposition on α7nAChR might be an aging related long-term process (Fig. 6A and B). And the AF incidence rate in APP/PS1 mice at 12 months old (7/10) was higher than those of WT mice and APP/PS1 mice at 3 and 6 months old (Supplementary Fig. 3A). Thus, 12-month-old WT and APP/PS1 mice were chosen in subsequent experiments in vivo. In order to precisely investigate the potential effects of α7nAChR on cardiomyocytes of aged WT or APP/PS1 mice, we specifically knocked down the expression of α7nAChR in cardiomyocytes by AAV-Chrna7 (Supplementary Figs. 3B–C). The Morris water maze test revealed remarkable cognitive deficits in APP/PS1 mice characterized by increased the escape latency and the time in target zone, which could not be reversed by AAV-Chrna7 (Fig. 6C, Supplementary Figs. 3D–G), indicating that the learning and memory ability of APP/PS1 mice was markedly weaker than that of WT mice no matter what kind of AAV transfection. In other words, AAV-Chrna7 did not apply to the brains and affect cognitive function. Therefore, compared to WT mice, AAV-Chrna7 successfully reduced the increased expression of α7nAChR, unfortunately not Aβ, in atria of APP/PS1 mice (Fig. 6D–F).

Among the groups, there were not differences in body weight (BW), systolic blood pressure (SBP), diastolic blood pressure (DBP), mean blood pressure (MBP), heart rate (HR), heart weight (HW) and heart weight/body weight (HW/BW) (Table .1), indicating that the mice in four groups exhibit same normal baseline phenotype. We assessed the cardiac function through echocardiographic analysis (Fig. 6G). The results demonstrated AAV-Chrna7 prevented the atrial dilation in APP/PS1 mice (Fig. 6H–J). However, there was no difference between WT and APP/PS1 mice with or without AAV-Chrna7 treatment in other echocardiographic parameters, including left ventricular internal diameter at end-diastole (LVIDd), left ventricular internal diameter at end-systole (LVIDs), ejection fraction (EF)(Fig. 6K-M). The atrial dysfunction in echocardiographic assays was in line with the structure remodeling characterized by increased fibrotic stain and total collagen level in APP/PS1 mice, which were suppressed by AAV-Chrna7 treatment (Fig. 6N–P). These data suggest that silencing α7nAChR of cardiomyocytes by AAV-Chrna7 treatment protects against APP/PS1 mutant-induced atrial structure remodeling.

3.6. Silencing α7nAChR blocked the high AF susceptibility and atrial electrical anomalies of APP/PS1 mice

To evaluate AF susceptibility, we carried out a transvenous burst pacing to induce atrial fibrillation. After programmed stimulation, compared to the WT + AAV-CON (1/10) and WT + AAV-Chrna7 (1/10) groups, a higher AF incidence were observed in the mice of APP/PS1+AAV-CON (7/10) group. which were attenuated by AAV-Chrna7 (3/10) (Fig. 7A and B). The AF duration of APP/PS1+ AAV-CON mice was significantly higher compared with the other three groups (Fig. 7C). These data indicated that APP/PS1 mice increased the AF susceptibility and persistency, which could be suppressed by silencing α7nAChR. Furthermore, in order to investigate the atrial electrical remodeling, we performed a protocol of the cardiac perfusion using nicotine, an α7nAChR agonist, or α-BTX, an α7nAChR antagonist. Electrophysiological mapping experiment showed that the atrial conduction velocity was markedly decreased by nicotine perfusion in the Langendorff-isolated hearts of WT. Surprisingly, nicotine did not significantly reduce the atrial conductivity of APP/PS1 mice, which might be due to the fact that both nicotine and Aβ act on α7nAChR, leading to a saturation effect. However, α-BTX resulted in increased atrial conductivity in both mice (Fig. 7D–F). As shown in Fig. 7E, ectopic pacing (black arrow) was shown in APP/PS1 group. The nicotine-induced upregulation of calculated dispersion was restrained by α-BTX in APP/PS1 isolated hearts, but not in WT group (Fig. 7G). These results indicate that inhibition of α7nAChR ameliorate electrical remodeling and reduces AF progression in APP/PS1 mice.

3.7. Silencing α7nAChR inhibited oxidative stress damage, apoptosis and inflammation in APP/PS1 mice, accompanied by down-regulated CaMKII oxidation and MAPK/AP-1 signaling pathway

We evaluated the effect of α7nAChR inhibition by AAV-Chrna7 on oxidative stress, apoptosis, and inflammation in WT and APP/PS1 mice. We found that AAV-Chrna7 exerted dramatically protective effect against APP/PS1-mutation induced mitochondrial oxidative damage as evidenced by reduced MitoSOX-Red fluorescence intensity (Fig. 8A and B). Increased TUNEL fluorescence intensity was shown in APP/PS1 mice, which could be reversed by AAV-Chrna7 (Fig. 8C and D). Moreover, measurement of atrial inflammatory cytokines exhibited higher TNF-α, IL-1, IL-6 and IL-10 levels in APP/PS1+AAV-CON group, compared to WT + AAV-CON and WT + AAV-Chrna7 groups, and these cytokines, not IL-10, could be reversed by AAV-Chrna7 (Fig. 8E–H). To further confirm the mechanism of Aβ/α7nAChR in signaling pathways, the key protein expression of CaMKII and related MAPK was examined. Western blotting analysis showed that AAV-Chrna7 treatment inhibited the APP/PS1 mutant-induced upregulation of oxi-CaMKII/CaMKII, p-p38/p38, p-Erk/Erk, c-Fos and c-Jun (Fig. 8I-Q). In summary, these results showed that silencing α7nAChR of cardiomyocytes suppressed APP/PS1 mutant-induced oxidative stress, apoptosis and inflammation by downregulating the activity and expression of CaMKII and MAPK/AP-1 signaling pathway.

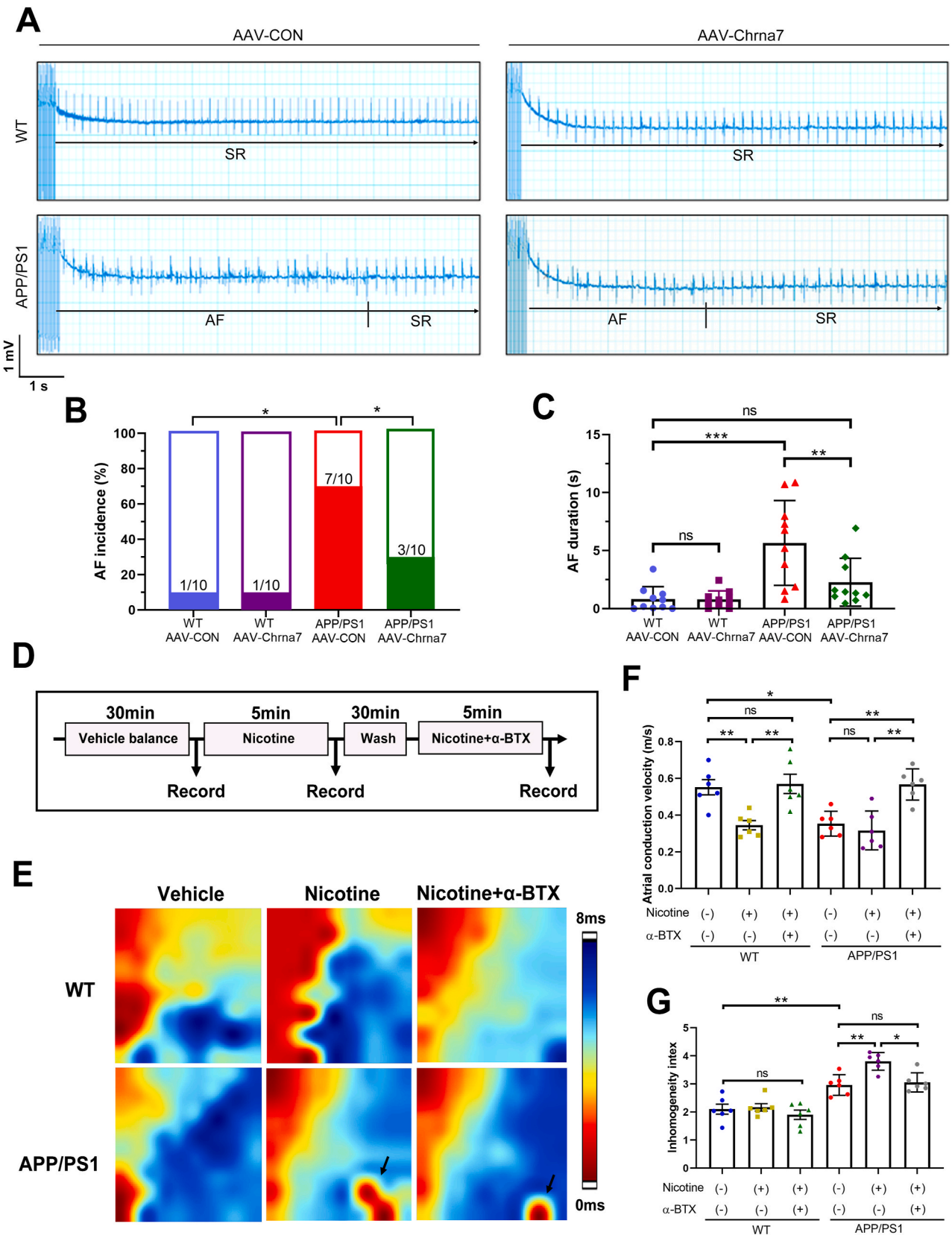

Fig. 7. Silencing α7nAChR blocked the high AF susceptibility and atrial electrical anomalies of APP/PS1 mice. (A) Representative electrocardiogram AF episodes induced by intra-atrial burst pacing. (B) Quantitative analysis of AF incidence (n = 10). (C) Quantitative analysis of AF duration (n = 10). (D) Schematic of the experimental design of epicardial electrical mapping recording. (E) Successive isochronal conduction maps of left atria of WT and APP/PS1 mice. Black arrow means ectopic pacing. (F) Quantitative analysis of atrial conduction velocity (n = 6). (G) Quantitative analysis of Inhomogeneity index (n = 6). Data were presented as Mean ± S.D. $^{ns}P > 0.05$, $^{*}P < 0.05$, $^{**}P < 0.01$ and $^{***}P < 0.001$.

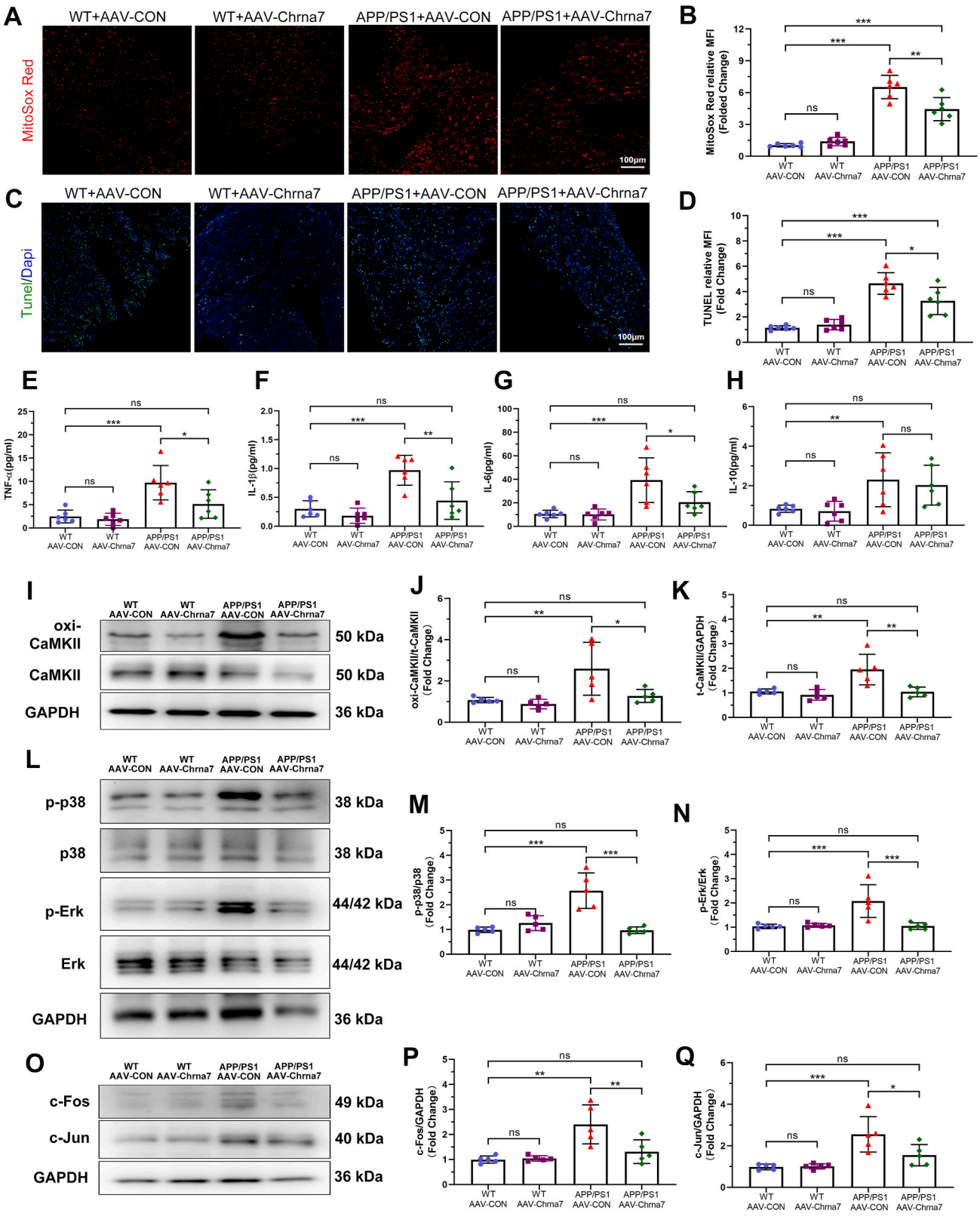

Fig. 8. Silencing α7nAChR inhibited oxidative stress damage, apoptosis and inflammation in APP/PS1 mice, accompanied by down-regulated CaMKII oxidation and MAPK/AP-1 signaling pathway. (A, B) Representative images and quantitative analysis of MitoSox (red) fluorescence in the atria of each group (n = 6). (C, D) Representative images and quantitative analysis of TUNEL (green) fluorescence in the atria of each group (n = 6). Quantifications of (E) tumor necrosis factor (TNF) -α, (F) interleukin (IL) -1β, (G) IL-6 and (H) IL-10 (n = 6). (I–K) Representative western blotting and quantitative analysis of oxi-CaMKII and CaMKII (n = 5). (L–N) Representative western blotting and quantitative analysis of p-p38/p38 and p-Erk/Erk (n = 5). (O–Q) Representative western blotting and quantitative analysis of c-Fos and c-Jun (n = 5). Data were presented as Mean ± S.D. $^{ns}P > 0.05$, $^{*}P < 0.05$, $^{**}P < 0.01$ and $^{***}P < 0.001$. Calibration bar = 100 μm. (For interpretation of the references to color in this figure legend, the reader is referred to the Web version of this article.)

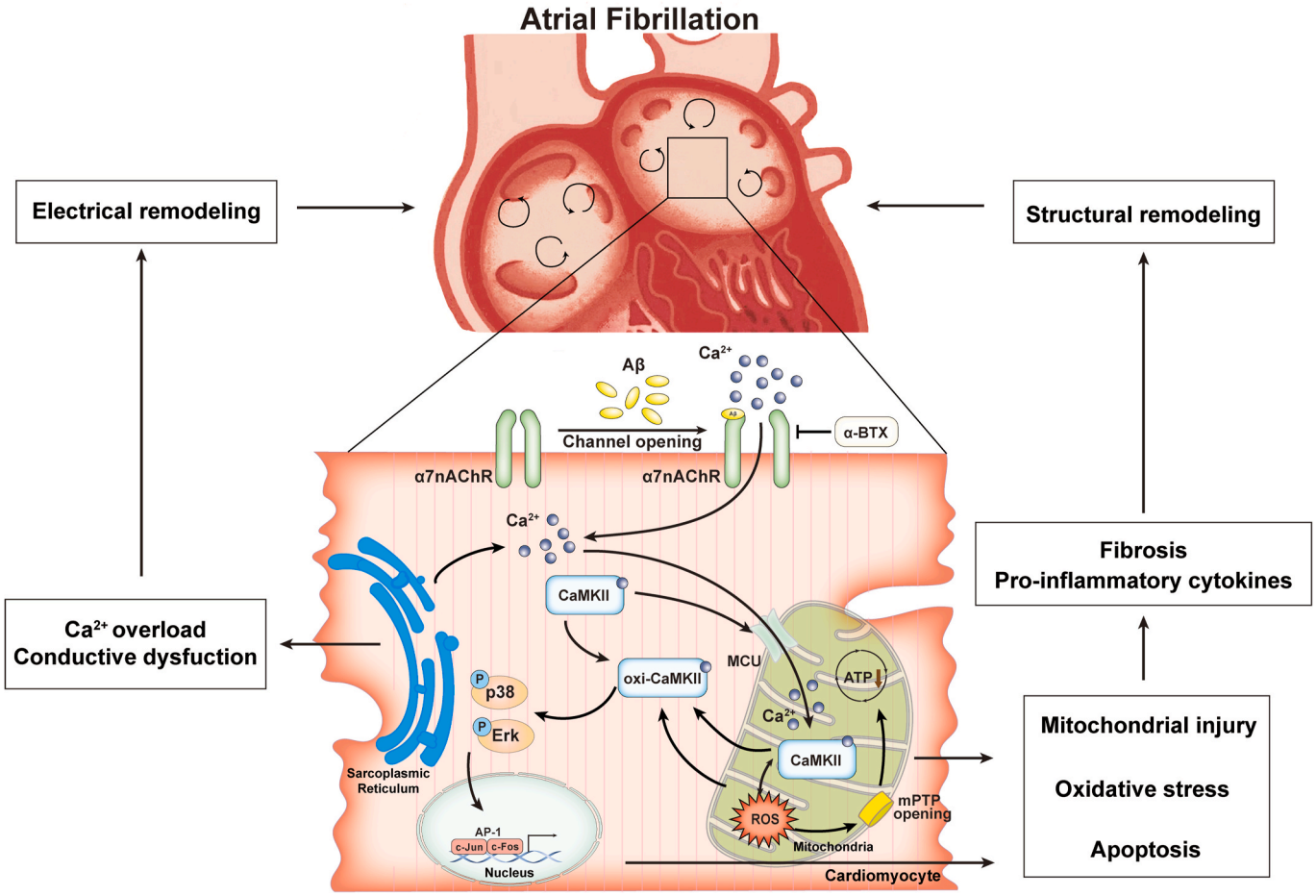

Fig. 9. A schematic illustration of the working model. The present study demonstrated that diminished α7 nicotinic acetylcholine receptor (α7nAChR) prevents amyloid-β (Aβ) induced mitochondrial oxidative stress and ameliorates atrial remodeling, by inhibiting oxi-CaMKII/MAPK/AP-1 signaling pathway.

4. Discussion

In present study, the core findings are as follows: 1) α7nAChR is upregulated in long-term treated HL-1 cells and atrial myocytes of late-stage AD mice; 2) α7nAChR deficiency in cardiomyocytes attenuates Aβ-induced oxidative stress and mitochondrial injury with Ca^{2+} mishandling in vitro; 3) Atrial remodeling and cardiac electrical dysfunction in APP/PS1 were ameliorated by specifically silencing α7nAChR in cardiomyocytes mediated by oxi-CaMKII/MAPK/AP-1 axis, thereby, preventing AF pathogenesis. Our study suggests that α7nAChR deficiency in cardiomyocytes may have a protection effect on Aβ-related AF pathogenesis (Fig. 9), To our knowledge, this is the first report to demonstrate the role of α7nAChR in the relationship between AD and AF.

AD is a neurodegenerative disease characterized by the obvious Aβ deposition and accumulation of neurofibrillary tangles [31]. Previous studies have shown that cardiac amyloidosis is associated with a high prevalence of AF [32,33]. A further study revealed that pathways of Aβ metabolic processes, Aβ formation and APP catabolic processes were activated in patients suffered from heart failure with concomitant AF [34], suggesting that Aβ deposition, as the marker of AD, also involved in pathophysiological processes of cardiac diseases. The pulmonary vein contains abundant amyloid peptides and directly influences atrial remodeling as a major substrate of AF [35]. Moreover, cardiac dysfunction of AD model mice and cytotoxicity of Aβ to cardiomyocytes have been reported [24,36,37]. Our study and others have reported that mitochondrial oxidative stress plays a pivotal role in the pathogenesis of both AD and AF [20,38], which could be attributed to Ca^{2+} overload, ROS generation and energy deprivation [39]. Importantly, we found that the adverse effects of Aβ on cardiomyocytes required a long-term accumulation both in vivo and vitro, which was consistent with the characteristics of AD and AF as senile diseases. Our data indicated the effect of Aβ-α7nAChR on cardiac dysfunction of late-stage AD model, however the targeted interruption of this ongoing worsening of cardiac dysfunction by Aβ need to be more investigated.

α7nAChR is a pentamer ligand gated ion channel, which plays a variety of signal transduction roles in human physiological functions [40]. α7nAChR has made a lot of progress in the research related to the improvement of cognitive function, and therapeutic effects of α7nAChR agonists on AD have been widely reported [41]. However, it has been reported that the activation of α7nAChR can promote the formation of fibrosis, atherosclerosis and right ventricular dysfunction [42,43]. Hence one can see that α7nAChR plays various, even contrary, functions on different types of cells and diseases. In order to avoid the interference of α7nAChR influencing on other types of cells in vivo, such as anti-inflammatory effect of α7nAChR on macrophages (cholinergic anti-inflammatory pathway, CAP) [44], an adeno-associated virus which specifically bound to cardiomyocytes was employed in present study. Our data demonstrated that silencing α7nAChR of cardiomyocytes reversed APP/PS1 mutant-induced atrial dysfunction and remodeling by suppressing ROS production, inflammation and apoptosis. Interestingly, silencing α7nAChR could successfully reverse the pro-inflammatory cytokines (TNF-α, IL-1β and IL-6), but not affect IL-10 in APP/PS1 mice. This different effect on pro- or anti-inflammatory factors might be related to diverse target pathways. IL-10 has strong anti-inflammatory properties and can block NF-κB activity, and mediated the regulation of JAK-STAT signal pathway [45].

The influences of IL-10 in ERK/MAPK pathway are indirect though inhibiting the expression of inflammatory factors such as TNF-α, IL-6 and IL-1. In addition, in present study, we found that reinstating Ca^{2+} load caused by inhibiting α7nAChR in Aβ-treated cardiomyocytes contributed to the beneficial effect, suggesting that the activation and opening of α7nAChR caused by Aβ led to Ca^{2+} influx, which gave rise to oxidative stress and mitochondrial injury. It is known that increasing the permeability of Ca^{2+} is the principal function of α7nAChR, which, in general, plays a positive biological effect (e.g., promoting synaptic plasticity and cognitive ability in hippocampal cells [46] or regulating polarization and phagocytosis in macrophages [47]). However, intracellular Ca^{2+} influx in cardiomyocytes can result in early or delayed afterdepolarization and spontaneous action potential, which trigger AF [48]. Interestingly, the effect of Aβ on α7nAChR increased the SR Ca^{2+} release and uptake, which promoted mitochondrial Ca^{2+} overload. The phenomenon could be caused by the CaMKII-mediated RYR2 and Serca2 dysfunction. The pseudo activation resulting from Aβ-α7nAChR induced membrane potential change may be another reason of the Ca^{2+} kinetics imbalance. Taken together with our findings, the effect of Ca^{2+} load might explain the pleiotropic roles of α7nAChR in diverse cell types and the poor uniformity of results of α7nAChR on cardiac function by pharmacological systemic administration in different studies [43,49]. Therefore, in terms of AD therapeutic drugs targeting activating α7nAChR, its side effects on cardiac function need to be paid full attention.

CaMKII is a multifunctional serine–threonine kinase as a pivotal connector of Ca^{2+} and ROS, which promote pluripotent signal for AF with atrial remodeling [21]. Recent studies revealed that CaMKII results in mPTP and MCU opening through the action of increasing mitochondrial Ca^{2+} and ROS, which leads to decreased ATP synthesis and apoptosis in cardiomyocytes [30,50]. In line with these findings, our data suggest that CaMKII, especially mitochondrial CaMKII, was involved in the effect of α7nAChR on Aβ-induced mitochondrial oxidative stress and atrial remodeling via MAPK/AP-1 signaling. Previous studies have proved that MAPK signaling pathways and AP-1 involved in fibrosis-related AF and the interaction between Aβ and α7nAChR [51–53]. Furthermore, here, we observed oxi-CaMKII induced by Ang II seems to play a more significant role in regulating MAPK pathway. It has been reported that oxi-CaMKII, as an activation of CaMKII, contributes to AF pathogenesis observed in both mice models and AF patients [54]. In fact, Wang et al. demonstrated that the overexpression and oxidation of CaMKII have a synergistic role in increasing the activity of CaMKII in the CaMKII arrhythmogenic mechanism [55]. We interpret these findings to support an important role for CaMKII as a transducer of Ca^{2+} and ROS in Aβ/α7nAChR-related AF.

5. Conclusion

In summary, we demonstrate, for the first time, that diminished α7nAChR of atrial myocytes plays a protective role against Aβ-induced mitochondrial oxidative stress and atrial remodeling, mediated by CaMKII/MAPK/AP-1 pathway. Importantly, our study provides a solid connection between AD and AF via α7nAChR, and highlight a new perspectives of targeting α7nAChR for elucidating the potential role of Aβ in cardiac dysfunction.

Sources of funding

This work was supported by the National Natural Science Foundation of China (grant number: 82070239) and Liaoning Provincial Natural Science Foundation (grant number: 2020JH2/10300156).

Declaration of competing interest

All authors declare no conflict of interest.

Data availability

No data was used for the research described in the article.

Appendix A. Supplementary data

Supplementary data to this article can be found online at https://doi.org/10.1016/j.redox.2022.102594.

References

[1] R. Proietti, A. AlTurki, R. Vio, L. Licchelli, F. Rivezzi, M. Marafi, V. Russo, T. S. Potpara, J.M. Kalman, E. de Villers-Sidani, T.J. Bunch, The association between atrial fibrillation and Alzheimer's disease: fact or fallacy? A systematic review and meta-analysis, J. Cardiovasc. Med. 21 (2) (2020) 106–112.
[2] T.J. Bunch, J.P. Weiss, B.G. Crandall, H.T. May, T.L. Bair, J.S. Osborn, J. L. Anderson, J.B. Muhlestein, B.D. Horne, D.L. Lappe, J.D. Day, Atrial fibrillation is independently associated with senile, vascular, and Alzheimer's dementia, Heart Rhythm 7 (4) (2010) 433–437.
[3] M. Di Nisio, M. Prisciandaro, A.W. Rutjes, I. Russi, L. Maiorini, E. Porreca, Dementia in patients with atrial fibrillation and the value of the Hachinski ischemic score, Geriatr. Gerontol. Int. 15 (6) (2015) 770–777.
[4] S. Kalantarian, T.A. Stern, M. Mansour, J.N. Ruskin, Cognitive impairment associated with atrial fibrillation: a meta-analysis, Ann. Intern. Med. 158 (5 Pt 1) (2013) 338–346.
[5] C.A. Papanastasiou, C.A. Theochari, N. Zareifopoulos, A. Arfaras-Melainis, G. Giannakoulas, T.D. Karamitsos, L. Palaiodimos, G. Ntaios, K.I. Avgerinos, D. Kapogiannis, D.G. Kokkinidis, Atrial fibrillation is associated with cognitive impairment, all-cause dementia, vascular dementia, and alzheimer's disease: a systematic review and meta-analysis, J. Gen. Intern. Med. 36 (10) (2021) 3122–3135.
[6] B. De Strooper, R. Vassar, T. Golde, The secretases: enzymes with therapeutic potential in Alzheimer disease, Nat. Rev. Neurol. 6 (2) (2010) 99–107.
[7] A. Poggesi, D. Inzitari, L. Pantoni, Atrial fibrillation and cognition: epidemiological data and possible mechanisms, Stroke 46 (11) (2015) 3316–3321.
[8] L. Troncone, M. Luciani, M. Coggins, E.H. Wilker, C.Y. Ho, K.E. Codispoti, M. P. Frosch, R. Kayed, F. Del Monte, Aβ amyloid pathology affects the hearts of patients with alzheimer's disease: mind the heart, J. Am. Coll. Cardiol. 68 (22) (2016) 2395–2407.
[9] P. Zimetbaum, Atrial fibrillation, Ann. Intern. Med. 166 (5) (2017) ITC33–ITC48.
[10] P.S. Chen, A.Y. Tan, Autonomic nerve activity and atrial fibrillation, Heart Rhythm 4 (3 Suppl) (2007) S61–S64.
[11] M.S. Dzeshka, G.Y. Lip, V. Snezhitskiy, E. Shantsila, Cardiac fibrosis in patients with atrial fibrillation: mechanisms and clinical implications, J. Am. Coll. Cardiol. 66 (8) (2015) 943–959.
[12] H.Y. Wang, D.H. Lee, M.R. D'Andrea, P.A. Peterson, R.P. Shank, A.B. Reitz, beta-Amyloid(1-42) binds to alpha7 nicotinic acetylcholine receptor with high affinity. Implications for Alzheimer's disease pathology, J. Biol. Chem. 275 (8) (2000) 5626–5632.
[13] K. Cao, Y.T. Dong, J. Xiang, Y. Xu, Y. Li, H. Song, W.F. Yu, X.L. Qi, Z.Z. Guan, The neuroprotective effects of SIRT1 in mice carrying the APP/PS1 double-transgenic mutation and in SH-SY5Y cells over-expressing human APP670/671 may involve elevated levels of α7 nicotinic acetylcholine receptors, Aging (Albany NY) 12 (2) (2020) 1792–1807.
[14] D. Puzzo, O. Arancio, Amyloid-β peptide: dr. Jekyll or Mr. Hyde? J. Alzheim. Dis. : JAD. 33 (1) (2013) S111–S120, 0 1.
[15] D. Puzzo, W. Gulisano, O. Arancio, A. Palmeri, The keystone of Alzheimer pathogenesis might be sought in Aβ physiology, Neuroscience 307 (2015) 26–36.
[16] E.X. Albuquerque, E.F. Pereira, M. Alkondon, S.W. Rogers, Mammalian nicotinic acetylcholine receptors: from structure to function, Physiol. Rev. 89 (1) (2009) 73–120.
[17] A. Vang, R.T. Clements, H. Chichger, N. Kue, A. Allawzi, K. O'Connell, E.M. Jeong, S.C. Dudley Jr., P. Sakhatskyy, Q. Lu, P. Zhang, S. Rounds, G. Choudhary, Effect of α7 nicotinic acetylcholine receptor activation on cardiac fibroblasts: a mechanism underlying RV fibrosis associated with cigarette smoke exposure, Am. J. Physiol. Lung Cell Mol. Physiol. 312 (5) (2017) L748–l759.
[18] N.C. Chang, C.T. Yeh, Y.K. Lin, K.T. Kuo, I.H. Fong, N.G. Kounis, P. Hu, M.Y. Hung, Garcinol attenuates lipoprotein(a)-induced oxidative stress and inflammatory cytokine production in ventricular cardiomyocyte through α7-nicotinic acetylcholine receptor-mediated inhibition of the p38 MAPK and NF-κB signaling pathways, Antioxidants 10 (3) (2021).
[19] Y. Zhao, B. Zhao, Oxidative stress and the pathogenesis of Alzheimer's disease, Oxid. Med. Cell. Longev. (2013), 316523, 2013.
[20] F.E. Mason, J.R.D. Pronto, K. Alhussini, C. Maack, N. Voigt, Cellular and mitochondrial mechanisms of atrial fibrillation, Basic Res. Cardiol. 115 (6) (2020) 72.
[21] O.O. Mesubi, M.E. Anderson, Atrial remodelling in atrial fibrillation: CaMKII as a nodal proarrhythmic signal, Cardiovasc. Res. 109 (4) (2016) 542–557.
[22] J. Beckendorf, M.M.G. van den Hoogenhof, J. Backs, Physiological and unappreciated roles of CaMKII in the heart, Basic Res. Cardiol. 113 (4) (2018) 29.
[23] A.V. Kuznetsov, S. Javadov, S. Sickinger, S. Frotschnig, M. Grimm, H9c2 and HL-1 cells demonstrate distinct features of energy metabolism, mitochondrial function

and sensitivity to hypoxia-reoxygenation, Biochim. Biophys. Acta 1853 (2) (2015) 276–284.
[24] S. Jang, X.R. Chapa-Dubocq, R.M. Parodi-Rullán, S. Fossati, S. Javadov, Beta-amyloid instigates dysfunction of mitochondria in cardiac cells, Cells 11 (3) (2022).
[25] L.-M. Yu, X. Dong, J.-K. Zhao, Y.-L. Xu, D.-Y. Xu, X.-D. Xue, Z.-J. Zhou, Y.-T. Huang, Q.-S. Zhao, L.-Y. Luo, Z.-S. Wang, H.-S. Wang, Activation of PKG-CREB-KLF15 by melatonin attenuates Angiotensin II-induced vulnerability to atrial fibrillation via enhancing branched-chain amino acids catabolism, Free Radic. Biol. Med. 178 (2022) 202–214.
[26] L.M. Yu, X. Dong, J.K. Zhao, Y.L. Xu, D.Y. Xu, X.D. Xue, Z.J. Zhou, Y.T. Huang, Q. S. Zhao, L.Y. Luo, Z.S. Wang, H.S. Wang, Activation of PKG-CREB-KLF15 by melatonin attenuates Angiotensin II-induced vulnerability to atrial fibrillation via enhancing branched-chain amino acids catabolism, Free Radic. Biol. Med. 178 (2022) 202–214.
[27] Z. Yin, H. Wang, Z. Wang, J. Han, Y. Zhang, H. Han, The midterm results of radiofrequency ablation and vagal denervation in the surgical treatment of long-standing atrial fibrillation associated with rheumatic heart disease, Thorac. Cardiovasc. Surg. 63 (3) (2015) 250–256.
[28] C. Jiao, F. Gao, L. Ou, J. Yu, M. Li, P. Wei, F. Miao, Tetrahydroxy stilbene glycoside (TSG) antagonizes Aβ-induced hippocampal neuron injury by suppressing mitochondrial dysfunction via Nrf2-dependent HO-1 pathway, Bio,ed. Pharmacother. 96 (2017) 222–228.
[29] L. Boyman, M. Greiser, W.J. Lederer, Calcium influx through the mitochondrial calcium uniporter holocomplex, MCU(cx), J. Mol. Cell. Cardiol. 151 (2021) 145–154.
[30] E.D. Luczak, Y. Wu, J.M. Granger, M.A. Joiner, N.R. Wilson, A. Gupta, P. Umapathi, K.R. Murphy, O.E. Reyes Gaido, A. Sabet, E. Corradini, W.W. Tseng, Y. Wang, A.J.R. Heck, A.C. Wei, R.G. Weiss, M.E. Anderson, Mitochondrial CaMKII causes adverse metabolic reprogramming and dilated cardiomyopathy, Nat. Commun. 11 (1) (2020) 4416.
[31] M. Yang, C. Li, Y. Zhang, J. Ren, Interrelationship between Alzheimer's disease and cardiac dysfunction: the brain-heart continuum? Acta Biochim. Biophys. Sin. 52 (1) (2020) 1–8.
[32] M. Grogan, C.G. Scott, R.A. Kyle, S.R. Zeldenrust, M.A. Gertz, G. Lin, K.W. Klarich, W.L. Miller, J.J. Maleszewski, A. Dispenzieri, Natural history of wild-type transthyretin cardiac amyloidosis and risk stratification using a novel staging system, J. Am. Coll. Cardiol. 68 (10) (2016) 1014–1020.
[33] M.P. van den Berg, B.A. Mulder, S.H.C. Klaassen, A.H. Maass, D.J. van Veldhuisen, P. van der Meer, H.L.A. Nienhuis, B.P.C. Hazenberg, M. Rienstra, Heart failure with preserved ejection fraction, atrial fibrillation, and the role of senile amyloidosis, Eur. Heart J. 40 (16) (2019) 1287–1293.
[34] B.T. Santema, V.A. Arita, I.E. Sama, M. Kloosterman, M.P. van den Berg, H.L. A. Nienhuis, I.C. Van Gelder, P. van der Meer, F. Zannad, M. Metra, J.M. Ter Maaten, J.G. Cleland, L.L. Ng, S.D. Anker, C.C. Lang, N.J. Samani, K. Dickstein, G. Filippatos, D.J. van Veldhuisen, C.S.P. Lam, M. Rienstra, A.A. Voors, Pathophysiological pathways in patients with heart failure and atrial fibrillation, Cardiovasc. Res. (2021).
[35] H.M. Tsao, P. Weerateerangkul, Y.C. Chen, Y.H. Kao, Y.K. Lin, J.H. Huang, S. A. Chen, Y.J. Chen, Amyloid peptide regulates calcium homoeostasis and arrhythmogenesis in pulmonary vein cardiomyocytes, Eur. J. Clin. Invest. 42 (6) (2012) 589–598.
[36] J. Murphy, T.N.V. Le, J. Fedorova, Y. Yang, M. Krause-Hauch, K. Davitt, L. I. Zoungrana, M.K. Fatmi, E.J. Lesnefsky, J. Li, D. Ren, The cardiac dysfunction caused by metabolic alterations in alzheimer's disease, Front Cardiovasc. Med. 9 (2022), 850538.
[37] S. Wang, L. Wang, X. Qin, S. Turdi, D. Sun, B. Culver, R.J. Reiter, X. Wang, H. Zhou, J. Ren, ALDH2 contributes to melatonin-induced protection against APP/PS1 mutation-prompted cardiac anomalies through cGAS-STING-TBK1-mediated regulation of mitophagy, Signal Transduct. Targeted Ther. 5 (1) (2020) 119.
[38] R. Parodi-Rullán, J.Y. Sone, S. Fossati, Endothelial mitochondrial dysfunction in cerebral amyloid angiopathy and alzheimer's disease, J. Alzheim. Dis. : JAD. 72 (4) (2019) 1019–1039.
[39] A.M. Aleardi, G. Benard, O. Augereau, M. Malgat, J.C. Talbot, J.P. Mazat, T. Letellier, J. Dachary-Prigent, G.C. Solaini, R. Rossignol, Gradual alteration of mitochondrial structure and function by beta-amyloids: importance of membrane viscosity changes, energy deprivation, reactive oxygen species production, and cytochrome c release, J. Bioenerg. Biomembr. 37 (4) (2005) 207–225.
[40] C.M. Noviello, A. Gharpure, N. Mukhtasimova, R. Cabuco, L. Baxter, D. Borek, S. M. Sine, R.E. Hibbs, Structure and gating mechanism of the α7 nicotinic acetylcholine receptor, Cell 184 (8) (2021), 2121-2134.e2113.
[41] J.L. Hoskin, Y. Al-Hasan, M.N. Sabbagh, Nicotinic acetylcholine receptor agonists for the treatment of alzheimer's dementia: an update, Nicotine Tob. Res. : Off. J. Soc. Res. Nicotine Tobacco 21 (3) (2019) 370–376.
[42] C. Heeschen, J.J. Jang, M. Weis, A. Pathak, S. Kaji, R.S. Hu, P.S. Tsao, F.L. Johnson, J.P. Cooke, Nicotine stimulates angiogenesis and promotes tumor growth and atherosclerosis, Nat. Med. 7 (7) (2001) 833–839.
[43] A. Vang, D. da Silva Gonçalves Bos, A. Fernandez-Nicolas, P. Zhang, A.R. Morrison, T.J. Mancini, R.T. Clements, I. Polina, M.W. Cypress, B.S. Jhun, E. Hawrot, U. Mende, O.U. J, G. Choudhary, α7 Nicotinic acetylcholine receptor mediates right ventricular fibrosis and diastolic dysfunction in pulmonary hypertension, JCI Insight 6 (12) (2021).
[44] D.B. Hoover, Cholinergic modulation of the immune system presents new approaches for treating inflammation, Pharmacol. Ther. 179 (2017) 1–16.
[45] S. Schülke, Induction of interleukin-10 producing dendritic cells as a tool to suppress allergen-specific T helper 2 responses, Front. Immunol. 9 (2018) 455.
[46] C.M. Hernandez, R. Kayed, H. Zheng, J.D. Sweatt, K.T. Dineley, Loss of alpha7 nicotinic receptors enhances beta-amyloid oligomer accumulation, exacerbating early-stage cognitive decline and septohippocampal pathology in a mouse model of Alzheimer's disease, J. Neurosci. : Off. J. Soc. Neurosci. 30 (7) (2010) 2442–2453.
[47] S. Zumerle, B. Calì, F. Munari, R. Angioni, F. Di Virgilio, B. Molon, A. Viola, Intercellular calcium signaling induced by ATP potentiates macrophage phagocytosis, Cell Rep. 27 (1) (2019) 1–10, e14.
[48] N. Voigt, N. Li, Q. Wang, W. Wang, A.W. Trafford, I. Abu-Taha, Q. Sun, T. Wieland, U. Ravens, S. Nattel, X.H. Wehrens, D. Dobrev, Enhanced sarcoplasmic reticulum Ca2+ leak and increased Na+-Ca2+ exchanger function underlie delayed afterdepolarizations in patients with chronic atrial fibrillation, Circulation 125 (17) (2012) 2059–2070.
[49] Y.H. Yang, H.L. Fang, M. Zhao, X.L. Wei, N. Zhang, S. Wang, Y. Lu, X.J. Yu, L. Sun, X. He, D.L. Li, J.J. Liu, W.J. Zang, Specific α7 nicotinic acetylcholine receptor agonist ameliorates isoproterenol-induced cardiac remodelling in mice through TGF-β1/Smad3 pathway, Clin. Exp. Pharmacol. Physiol. 44 (12) (2017) 1192–1200.
[50] F. Fieni, D.E. Johnson, A. Hudmon, Y. Kirichok, Mitochondrial Ca2+ uniporter and CaMKII in heart, Nature 513 (7519) (2014) E1–E2.
[51] D. Li, K. Shinagawa, L. Pang, T.K. Leung, S. Cardin, Z. Wang, S. Nattel, Effects of angiotensin-converting enzyme inhibition on the development of the atrial fibrillation substrate in dogs with ventricular tachypacing-induced congestive heart failure, Circulation 104 (21) (2001) 2608–2614.
[52] K.W. Chang, H.F. Zong, K.G. Ma, W.Y. Zhai, W.N. Yang, X.D. Hu, J.H. Xu, X. L. Chen, S.F. Ji, Y.H. Qian, Activation of α7 nicotinic acetylcholine receptor alleviates Aβ(1-42)-induced neurotoxicity via downregulation of p38 and JNK MAPK signaling pathways, Neurochem. Int. 120 (2018) 238–250.
[53] K.G. Ma, J. Lv, W.N. Yang, K.W. Chang, X.D. Hu, L.L. Shi, W.Y. Zhai, H.F. Zong, Y. H. Qian, The p38 mitogen activated protein kinase regulates β-amyloid protein internalization through the α7 nicotinic acetylcholine receptor in mouse brain, Brain Res. Bull. 137 (2018) 41–52.
[54] E.D. Luczak, M.E. Anderson, CaMKII oxidative activation and the pathogenesis of cardiac disease, J. Mol. Cell. Cardiol. 73 (2014) 112–116.
[55] W. Wang, W. Shen, S. Zhang, G. Luo, K. Wang, Y. Xu, H. Zhang, The role of CaMKII overexpression and oxidation in atrial fibrillation-A simulation study, Front. Physiol. 11 (2020), 607809.